



HAL
open science

Aeroacoustics research in Europe: The CEAS-ASC report on 2018 highlights

Denis Gély, Gareth Bennett

► **To cite this version:**

Denis Gély, Gareth Bennett. Aeroacoustics research in Europe: The CEAS-ASC report on 2018 highlights. *Journal of Sound and Vibration*, 2019, 463, pp.114950. 10.1016/j.jsv.2019.114950 . hal-02863997

HAL Id: hal-02863997

<https://hal.science/hal-02863997>

Submitted on 24 Jul 2020

HAL is a multi-disciplinary open access archive for the deposit and dissemination of scientific research documents, whether they are published or not. The documents may come from teaching and research institutions in France or abroad, or from public or private research centers.

L'archive ouverte pluridisciplinaire **HAL**, est destinée au dépôt et à la diffusion de documents scientifiques de niveau recherche, publiés ou non, émanant des établissements d'enseignement et de recherche français ou étrangers, des laboratoires publics ou privés.

Aeroacoustics research in Europe: The CEAS-ASC report on 2018 highlights

Denis Gely^a, Gareth J. Bennett^{b,*}

^aDAAA, Aerodynamics, Aeroelasticity, Acoustics Department, ONERA - The French Aerospace Lab, BP 72 - 29 Avenue de la Division Leclerc, 92322 Châtillon, France

^bDepartment of Mechanical and Manufacturing Engineering, School of Engineering, Trinity College Dublin, the University of Dublin, D02 PN40, Ireland

Abstract

The Council of European Aerospace Societies (CEAS) Aeroacoustics Specialists Committee (ASC) supports and promotes the interests of the scientific and industrial aeroacoustics community on an European scale and European aeronautics activities internationally. In this context, “aeroacoustics” encompasses all aerospace acoustics and related areas. Each year the committee highlights some of the research and development projects in Europe.

This paper is a report on highlights of aeroacoustics research in Europe in 2018, compiled from information provided to the ASC of the CEAS. During 2018, a number of research programmes involving aeroacoustics were funded by the European Commission. Some of the highlights from these programmes are summarised in this article, as well as highlights from other programmes funded by national programmes or by industry. Furthermore, a concise summary of the CEAS-ASC workshop “Future Aircraft Design and Noise Impact” held in the Netherlands Aerospace Centre (NLR) Amsterdam in September 2018 is included in this report.

Enquiries concerning all contributions should be addressed to the authors who are given at the end of each subsection.

1. CEAS-ASC workshop

The 22nd CEAS-ASC Annual Scientific Workshop was held in NLR Amsterdam, on September 6-7, 2018. Its topic was “Future Aircraft Design and Noise Impact” and it was organized by Harry Brouwer of NLR and in co-operation with the EU project ANIMA (Aviation Noise Impact Management through Novel Approaches). The focus of the workshop was on the relationship between aircraft design and noise impact. Contributions were invited from both the domains of technology and impact assessment and thus the overarching objective of the workshop was to encourage discussion and cooperation between researchers in low noise technologies on one hand and on noise impact assessment and mitigation on the other.

Topics on which contributions were invited included: ◦ Aircraft overall noise ◦ Noise propagation ◦ Auralization ◦ Noise impact of new architectures ◦ Boundary layer ingestion ◦ Distributed

*Corresponding author. Tel.: +353 1 896 1383

Email address: gareth.bennett@tcd.ie (Gareth J. Bennett)

Preprint submitted to *Journal of Sound and Vibration*

June 18, 2019

12 propulsion ◦ Single event models ◦ Metrics ◦ From wind tunnel data to noise impact assessment
13 ◦ Noise impact of drones ◦ Non-acoustical factors

14 A total of 33 abstracts were received, 27 of which were accepted by the workshop scientific
15 committee. In addition, 4 researchers accepted an invitation to present a keynote overview :

- 16 • Lothar Bertsch, DLR: 10 years of joint research at DLR and TU Braunschweig toward low-
17 noise aircraft design - what did we achieve?
- 18 • Russell Thomas, NASA: Realizing NASAs Vision for Low Noise Subsonic Transport Air-
19 craft.
- 20 • Infrid Legriffon & Laurent Sanders, ONERA: Single Event Noise Prediction at ONERA -
21 Case of aircraft powered by contra-rotating open rotors.

22 The workshop was well-attended with 56 participants from 13 European countries and the
23 USA. The participation from the USA was somewhat larger then on previous occasions with 6
24 participants from NASA, FAA, and Pennsylvania State University. Proceedings can be found at
25 <https://www.nlr.org/ceas-asc-2018-workshop/>.

26 **2. Airframe noise**

27 *2.1. Numerical study of fan noise installation effects using the Immersed Boundary Method*

28 For several years, ONERA has been developing an innovative two-step CFD/CAA workflow
29 based on solid surfaces described by unstructured meshes immersed in volume Cartesian grids.
30 This so-called Immersed Boundary Method (IBM) is particularly efficient to evaluate acoustic
31 engine installation effects on novel aircraft architectures. The methodology consists in, first,
32 computing the mean flow around the geometry of interest with the CFD solver FastS [1], then
33 use the CAA solver sAbrinA_{v0} [2] to compute the propagation of acoustic waves generated by
34 any kind of noise source. Both solvers are used in Cartesian mode, and have their IBM pre-
35 process based on the Cassiopee package [1]. The method allows to drastically reduce the mesh
36 design efforts as well as the computational costs for both CFD and CAA stages. First validations
37 of the methodology with no mean flow confirmed its efficiency and reliability [3].

38 This methodology has been successfully applied to study the installation effects, on the
39 fan/OGV interaction noise, of two different implementations OWN and UWN (Over- and Under-
40 Wing-Nacelle) of classic turbofans on ONERAs NOVA aircraft, accounting for realistic non-
41 uniform mean flows at $M = 0.25$ (i.e. take-off/landing flight conditions). Instantaneous pressure
42 fluctuations computed by the sAbrinA_{v0} solver are plotted in Fig. 1. for the two configurations.
43 Multiple interference patterns, mainly due to reflection/scattering effects on the solid surfaces
44 and refraction effects due to the mean flow gradients, are clearly noticeable. The comparison of
45 noise maps on the ground (see Fig. 2) shows that the OWN configuration brings noise reduc-
46 tion of more than 15 dB, especially in front of the aircraft as could be expected from this noise
47 shielding effect.

48 These simulations demonstrate the capacities of the present numerical workflow. Parametric
49 studies, dealing with acoustic efficiency for installation effects, are now affordable.



Figure 1: Instantaneous pressure fluctuations with one-sided engine aircraft in the vertical nacelle mid-section plane: UWN configuration (left); OWN configuration (right).

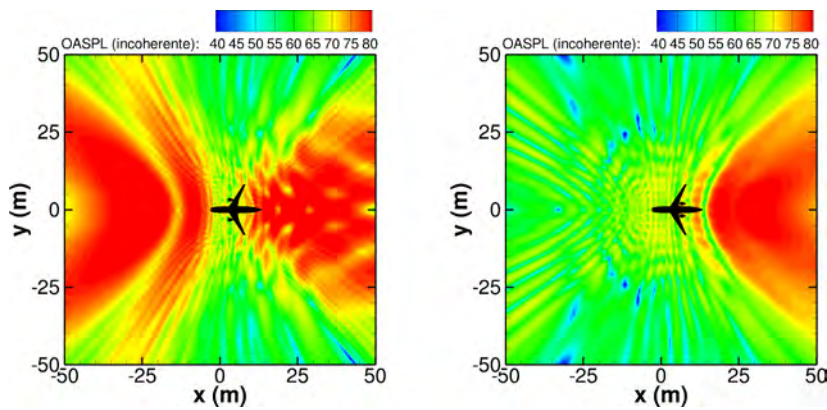


Figure 2: Extrapolated acoustical pressure maps (in dB) with a two-sided engine aircraft: UWN configuration (left); OWN configuration (right)

50 *Written by Mathieu Lorteau: mathieu.lorteau@onera.fr, Ludovic Wiert, Thomas Le Garrec, ON-*
 51 *ERA, France*

52 **Submission Country: France**

53 *2.2. The Air Curtain as a Fluidic Spoiler to Reduce Aerodynamic Noise.*

54 The air curtain has been used in a number of diverse engineering applications, such as acting as
 55 smoke, heat or contamination barriers. In aeronautics, it was first proposed for use for landing-
 56 gear noise reduction by Wickerhoff and Sijpkens [4], after which Oerlemans and de Bruin [5]
 57 performed proof-of-concept research to validate it on a generic bluff body. In recent years, the
 58 planar jet as a means to reduce noise has been further investigated and advanced by Zhao et al.
 59 [6, 7], in which tandem rods were examined as a simplified representation of aircraft landing gear.
 60 Subsequently, in order to minimise the additional noise source introduced by the air curtain itself,
 61 the dual air curtain has been developed and investigated, in which improved acoustic and energy
 62 efficiency have been achieved through the addition of a second upstream planar jet [8, 9]. Initial
 63 research has been conducted into the development of the Fluidic Spoiler as a landing gear noise
 64 reduction technology beyond representative academic configurations, see Fig 3. In addition to
 65 the acoustical studies, the fluid mechanics of dual planar jets in a cross flow, which have received
 66 little attention in the literature, have been extensively examined with PIV, hotwire and numerical

67 analysis, and proper orthogonal decomposition has been performed in order to characterise the
 68 coherent structures of the flow field, particularly the large-scale vortices mainly occurring in the
 69 shear layers [10, 11, 12]. Further applications of the air curtain, also called: Fluidic Spoiler, have
 70 been studied such as the use of the air curtain to shield the aerodynamic noise of the pantograph
 71 of a high speed train or to reduce cavity noise [13], see Fig 4.

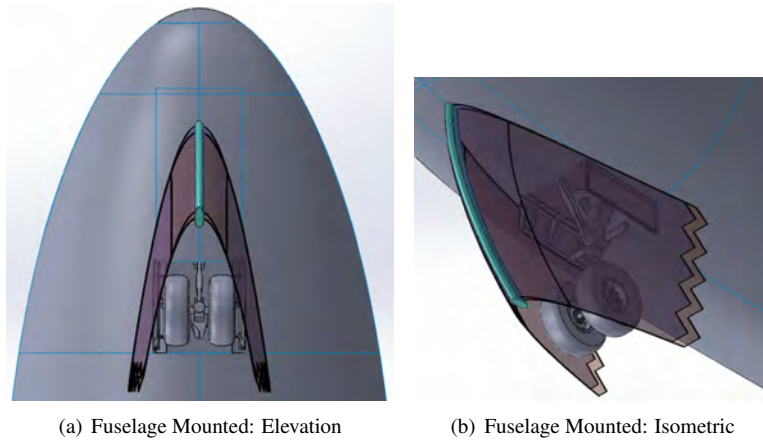


Figure 3: Dual-jet air curtain concept for shielding nose landing gear. Not to scale.

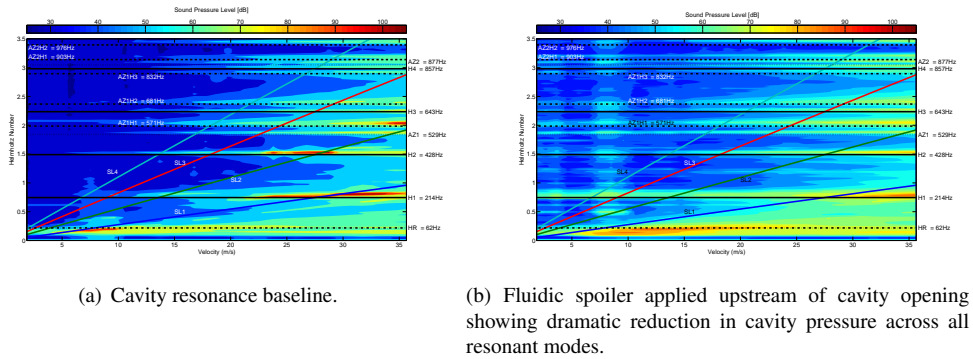


Figure 4: Sound pressure level [dB] inside a cylindrical cavity as a function of tunnel flow-speed. Superimposed on the plot are the theoretical shear layer modes (SL), the theoretical acoustic resonant modes, including azimuthal, (H1, AZ1...), and the Helmholtz resonance (HR).

72 *Written by Kun Zhao: kzhao@tcd.ie, Trinity College Dublin, the University of Dublin.*
 73 **Submission Country: Ireland**

74 **2.3. Full Scale Nose Landing Gear Analysis.**

75 Recently research has been published based on the experimental results from the Clean Sky
 76 funded ALLEGRA Advanced LowNoise Landing (Main and Nose) Gear for Regional Aircraft

77 project. This project was developed to assess low-noise technologies applied to a full-scale
78 nose landing gear model and a half-scale main landing-gear model of a 90-seat configuration
79 regional aircraft concept. With regard to the nose landing gear (NLG) campaign, one of the
80 significant contributions of ALLEGRA is that a complete and highly detailed representation of
81 the landing-gear components and associated structures such as the complete wheel bay cavity
82 (wheel well), bay doors, nose fuselage and hydraulic dressings were included at full scale [14,
83 15, 16]. In 2018, results from a decomposition analysis was performed where LG components
84 were removed one after the other in order to assess their individual contribution [17]. In addition,
85 low noise treatments such as wheel hub caps, retractable fuselage fairings, perforated fairings and
86 wire mesh was evaluated, see Fig. 5. Additional interesting findings such as the excitation and
87 radiation of wheel well noise was assessed, in particular the higher order modes of the large
88 volume wheel well which can be excited within the velocity range of a landing aircraft[18];
89 modes that are usually ignored[19]. Also in 2018, windtunnel results were compared to flyover
90 results of real aircraft of a similar size and design as well as to standard semi-empirical models.
91 Particularly novel was the comparison to acoustic data extracted from CFD flow computations
92 which was propagated to simulated microphone arrays and processed using several beamforming
93 approaches [20]. Similar analyses were performed for the half scale MLG which also was found
94 to radiate noise from the wheel bay [21, 22].

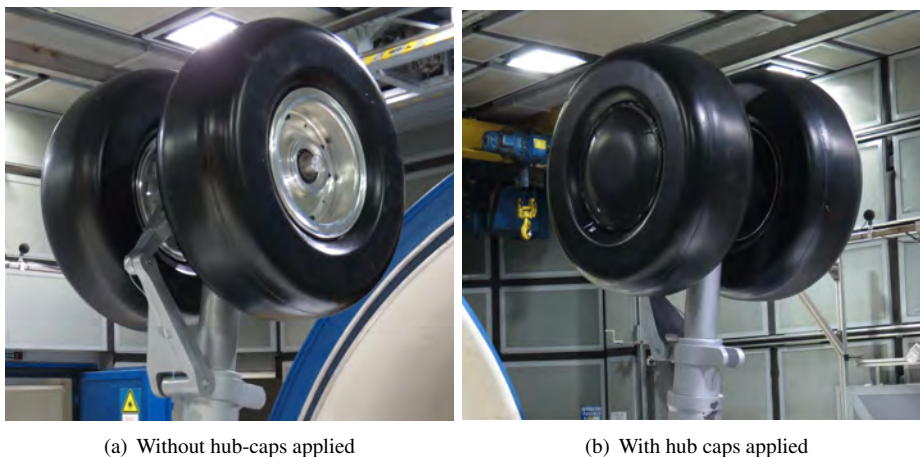


Figure 5: Hub-caps low noise technology applied to nose landing gear.

95 *Written by John Kennedy: kennedj@tcd.ie, Trinity College Dublin, the University of Dublin.*
96 *Ireland*

97 **Submission Country: Ireland**

98 2.4. *Retro-Fit Noise Reduction Technology Assessment through Flyover Noise Measurements*

99 The teams of the DLR Technical Acoustics and Engine Acoustics Departments achieved flight
100 tests with the DLR Airbus A320 research aircraft ATRA (Fig. 6). The aim of this combined
101 effort was to demonstrate the effect of selected retro-fit noise reductions means on the wings,
102 landing gears and the engine exhaust nozzles. The measurements were taken at Cochstedt airport

103 in Saxony-Anhalt (Germany) with a phased microphone array for source localization (Fig. 7,
 104 left) and widely distributed single farfield microphones in order to obtain absolute levels and
 105 directivity information. The tested porous flap side edge provided a 2 dB noise reduction in
 106 terms of the measured sound exposure level during flyover in about 600 ft height above the
 107 microphone in gear-up configuration. Selected fairings on both the main and nose landing gear
 108 showed a 1 - 2 dB noise reduction which strongly depends on the flight speed and high-lift system
 109 configuration. Noise reductions are very weak at high flap settings with potentially high gear-
 110 wake flap interaction noise generation. This result indicates that both sources need to be addressed
 111 together. The engine nozzle trailing edge modification leads to a high frequency noise reduction
 112 (Fig. 7, right) combined with the suppression of tonal engine noise components. The flight
 113 test was a core activity of the DLR project Low Noise ATRA. Contributions were made by the
 114 industrial partners Airbus and Safran.



Figure 6: ATRA approaching the measurement systems.

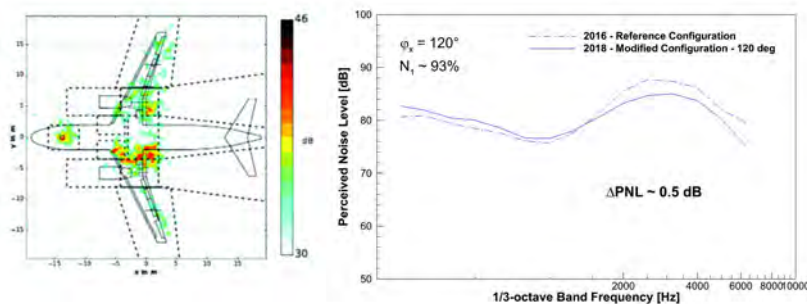


Figure 7: Source map for a fly-over in landing configuration calculated with a hybrid deconvolution method (left) and effect of the nozzle modification on the perceived noise level (right)

115 *Written by M.Pott-Pollenske: michael.pott-pollenske@dlr.de, H.Siller, DLR, Germany.*

116 **Submission Country: Germany**

117 *2.5. Numerical Analysis of the Impact of Variable Porosity on Trailing-Edge Noise*

118 The impact of permeability on the trailing-edge noise is analyzed by a constant and a variable
119 porous surface [23]. Porous media generate the Darcy drag force, i.e., the viscous effect of the
120 micro-structure inside a porous medium, which is numerically determined by the permeability
121 and the Forchheimer term. The permeability and the porosity of a baseline configuration are
122 defined based on the acoustic intensity quantified for various porous surfaces [24]. A variable
123 porous medium at a trailing edge is designed by an adjoint-based optimization. The constant
124 and the variable porous medium are applied to two flow configurations, one at zero deg. and
125 one at two deg. angle-of-attack (AOA), to indicate the impact of various loads on the suction
126 and pressure sides on the effectiveness of porous surfaces. In Fig 8 the directivity determined
127 by the overall sound pressure level is presented. The zero deg. AOA configuration shows that
128 the porous media reduce the noise generation independently from the direction. The acoustic
129 gain is determined by an induced drag force which leads to a lower convection velocity for the
130 turbulent flow passing over the trailing edge. The porous surface is extremely effective to reduce
131 the tone and the broadband noise [24]. The variable porosity configuration shows with the thick
132 arrows an additional noise reduction compared to the constant porosity medium. However, at two
133 deg. AOA the porous surface shows a lower impact on the noise reduction such that the acoustic
134 gain, which is obtained by the optimization at zero deg. AOA, is diminished. This sensitivity of
135 the porous-media effectiveness means that in future optimization approaches the AOA should be
136 considered an optimization parameter.

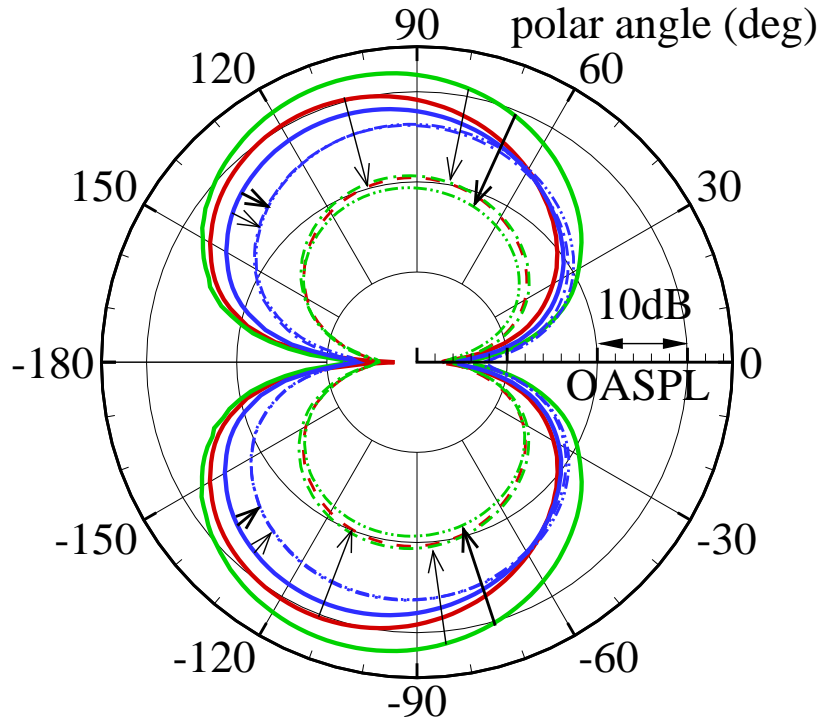


Figure 8: Overall sound pressure level determined by the acoustic perturbation equations black arrows indicate the noise reduction between impermeable (solid lines) and porous (dashed lines) surfaces color denotes the rounded (red) and the sharp (green) trailing-edge at zero deg. AOA and the rounded trailing-edge at two deg. AOA (blue).

137 *Written by Seong-Ryong Koh: s.koh@aia.rwth-aachen.de, Matthias Meinke, Wolfgang*
 138 *Schroeder, RWTH Aachen University, Germany, Beckett Zhou, Nicolas Gauger, TU-*
 139 *Kaiserslautern, Germany.*

140 **Submission Country: Germany**

141 *2.6. RANS-based trailing-edge noise prediction using Amiet's theory*

142 Amiet's semi-analytical model [25] for trailing-edge noise prediction was performed by cou-
 143 pling it with Reynolds-Averaged Navier-Stokes (RANS) simulations which are used to determine
 144 the wall-pressure statistics. Two families of wall-pressure spectrum models are compared: i)
 145 based on a resolution of the Poisson equation by integrating velocity statistics over the boundary
 146 layer thickness (Panton & Linebarger model [26]), or ii) directly addressing wall-pressure statis-
 147 tics through ad-hoc empirical models calibrated on experimental databases (Goody, Rozenberg,
 148 Kamruzzaman, Catlett, Hu & Herr and Lee models [27]). As illustrative test cases, two different
 149 configurations are treated in this work: a NACA0012 airfoil at 0 degree angle of attack (a.o.a)
 150 and a DU96-W-180 airfoil at 4 degrees a.o.a, the key differences between both cases being the
 151 importance of the wall-pressure gradient and symmetry between the pressure and suction sides.
 152 The results, see Fig. 9, indicate that both the semi-empirical model developed for adverse pres-
 153 sure gradients and the integral model yield good predictions for the NACA0012 test case. For the

154 Du96-W-180 airfoil, the Lee model which is modified for high adverse pressure gradient flow
 155 performs in the range of $\pm 3dB$. The Kamruzzaman model also exhibits a good performance in
 156 the range of ± 3 dB by considering its simple formulation. Lastly, Panton & Linebarger model
 157 predicts well the middle range whereas under-predicts around 2 dB for the higher frequencies.

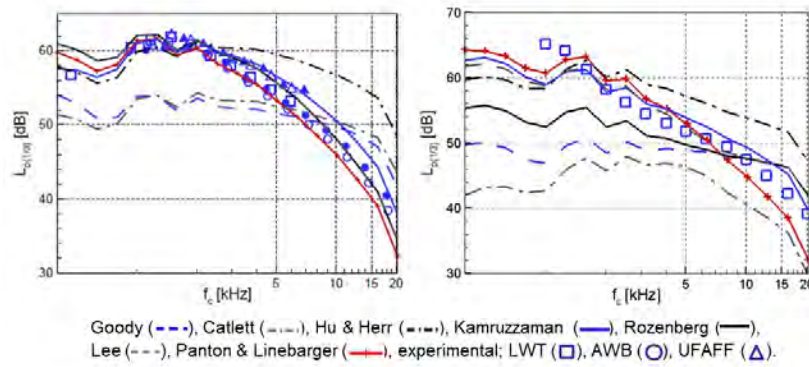


Figure 9: Far-field noise prediction by Amiet's theory with different wall-pressure models and comparison with an experimental data the NACA0012 airfoil (left) and the DU96-W-180 airfoil (right).

158 *Written by Y.C.Küçükosman: yakut.cansev.kucukosman@vki.ac.be, J. Christophe and C.*
 159 *Schram, von Karman Institute for Fluid Dynamics, Belgium*

160 **Submission Country: Belgium**

161 *2.7. The attenuation of the cavity tones induced by a low-speed flow using micro-perforated*
 162 *panels*

163 Experimental studies have been carried out to assess the effect on the pressure fluctuations
 164 of micro-perforating [28] the base wall of cavities mounted in a low-speed wind-tunnel and
 165 undergoing a fully-developed turbulent boundary layer [29], as shown in Fig 10. This passive
 166 strategy has hardly been studied in shallow cavities in transitional flow regime, e.g. with a
 167 length-to-depth ratio of about 10. The wall-pressure spectra acquired at Mach number 0.09
 168 over the cavity base panel showed dominant peaks on one third of the cavity floor towards the
 169 leading edge. Broadband pressure fluctuations dominate further downstream, with amplitudes
 170 of about 10 dB above that of the first peak. The peaks are identified as transverse tunnel-cavity
 171 resonances excited by the shear layer and coupled with the thin panel flexural modes. It can
 172 be seen from Fig 10 that micro-perforating the floor of the cavity reduces by up to 8 dB the
 173 dominant tonal peaks. This was also observed for a closed-flow cavity, but to a lesser extent.
 174 However, the micro-perforations are inefficient downstream of the reduction zone to attenuate
 175 the broadband pressure fluctuations, which can even be enhanced. Two-dimensional Lattice-
 176 Boltzmann simulations were performed for a transitional cavity mounted in a waveguide and
 177 undergoing a low-speed boundary layer. The calculated wall pressure spectra confirmed the
 178 existence of transverse tunnel-cavity resonances as well as their attenuation at the base and at the
 179 mouth of the cavity by inserting a micro-perforated floor. The dissipation of energy was found
 180 to be concentrated within and at the inlet-outlet of the base-wall apertures which correspond to

181 regions of maximum velocity fluctuations. A strategy would be to microperforate only part of
 182 the base wall that extends over one third of the cavity length in order to achieve attenuation of
 183 the dominant peaks without enhancement of the broadband wall-pressure fluctuations.

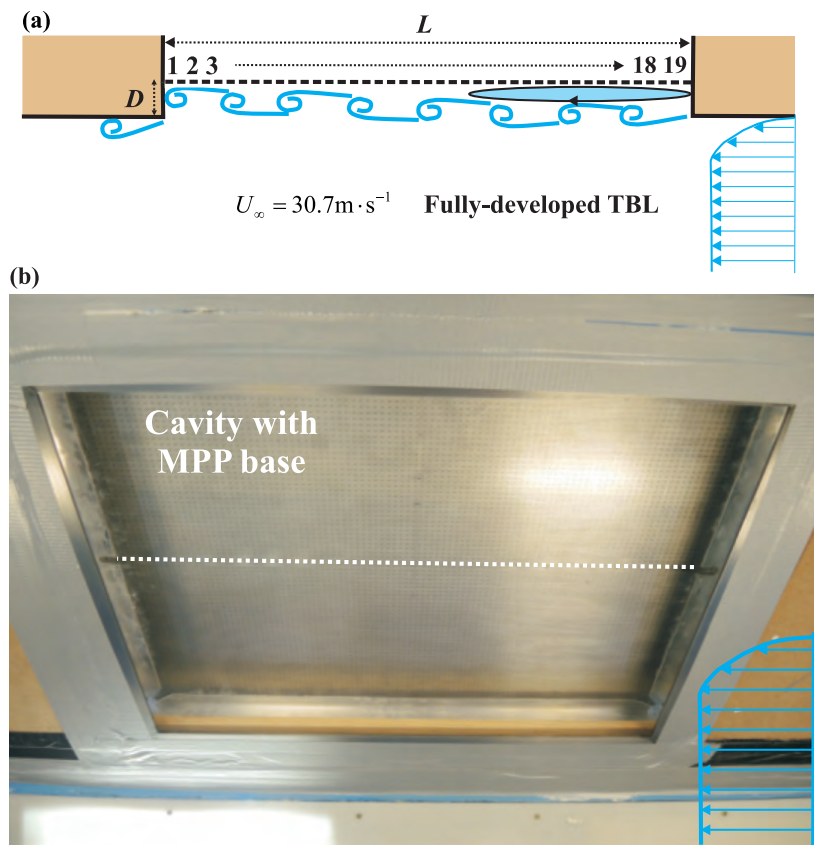


Figure 10: Views of a transitional flow cavity with micro-perforated base wall beneath a fully developed turbulent boundary layer: (a) sketch of the cavity with numbering of the 19 wall-pressure measurements positions evenly distributed over the centered length line of the base wall (b) photograph of the wind tunnel test section on top of which is mounted the micro-perforated cavity.

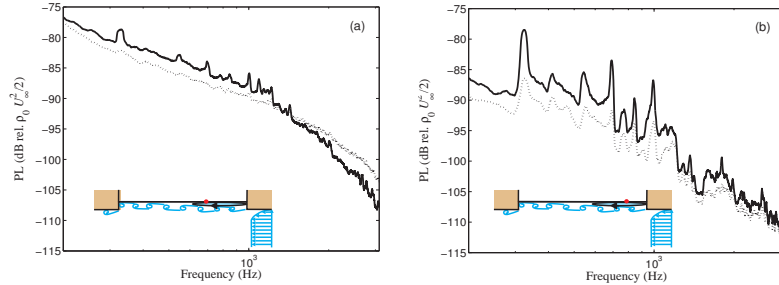


Figure 11: Effect of a microperforated floor on the pressure level (PL) spectra measured over the base wall of a transitional cavity with length-to-depth ratio 10.6: (a) at 18.2 cm and (b) at 9.8 cm from the cavity upstream edge. The solid curves correspond to a plain floor and the dotted curves to a microperforated floor the red dot in the sketches shows the measurement location.

184 *Written by Teresa Bravo (teresa.bravo@csic.es), Instituto de Tecnologías Físicas y de la Infor-*
 185 *mación, Consejo Superior de Investigaciones Científicas (CSIC), Serrano 144, 28006 Madrid,*
 186 *Spain, and Cédric Maury, Laboratoire de Mécanique et d'Acoustique, UMR 7031 AMU-CNRS-*
 187 *Centrale Marseille, 4 impasse Nikola Tesla, 13013 Marseille, France*

188 **Submission Country: Spain, France**

189 2.8. Airfoil noise reduction with add-ons and permeable materials

190 Leading-edge-impingement (LEI) noise and turbulent-boundary-layer trailing-edge (TBL-TE)
 191 noise are amongst the most relevant sources for airframe and turbofan noise (i.e., rotor/stator in-
 192 teraction noise). They can be mitigated by using serrations or reducing the pressure imbalance
 193 with permeable surfaces. Recent developments have confirmed that serrations reduce noise by
 194 generating destructive interference between the scattered pressure waves for both TBL-TE and
 195 LEI noise. For TBL-TE noise [30], it has been proven that the effect of the serrations on the flow
 196 is to increase the spanwise coherence of the turbulent structures, which promotes destructive
 197 interference for slanted edges. This is achieved by altering the flow features over the serration
 198 surface, see Fig. 12, both the size of the turbulent structures and their convective direction, as
 199 also proved experimentally [31]. Conversely, for rotor/stator impingement noise [32], the di-
 200 mensions of the turbulent structures in the slipstream of the fan is such that, to realise destructive
 201 interference and to reduce noise more than 1 dB, large amplitude serrations are necessary, thus
 202 affecting negatively both the aerodynamic performances and robustness of the stator. An alter-
 203 native approach to reduce noise is the application of permeable surfaces at both the leading and
 204 trailing edge. In this case, the noise reduction mechanism is the reduction of the pressure imbal-
 205 ance. For TBL-TE noise [33], permeable materials have been shown to reduce noise up to 10 dB
 206 in wind tunnel applications. It has been proven that the conventional model adopted for a solid
 207 trailing edge cannot be applied for porous materials because additional noise sources are present.
 208 Conversely, for LIN [34], the adoption of a permeable surface at the leading edge has shown that
 209 the presence of flow through the insert that forces transition to turbulence, see Fig. 13. In this
 210 case, alleviation of LEI noise has been obtained but with an increase of TBL-TE.

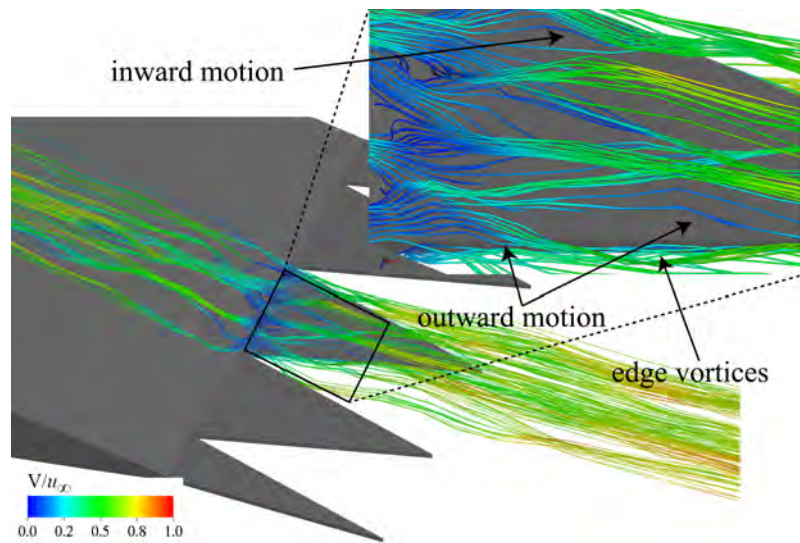


Figure 12: Streamlines representing the instantaneous flow field over a serrated trailing edge obtained with the lattice-Boltzmann method.

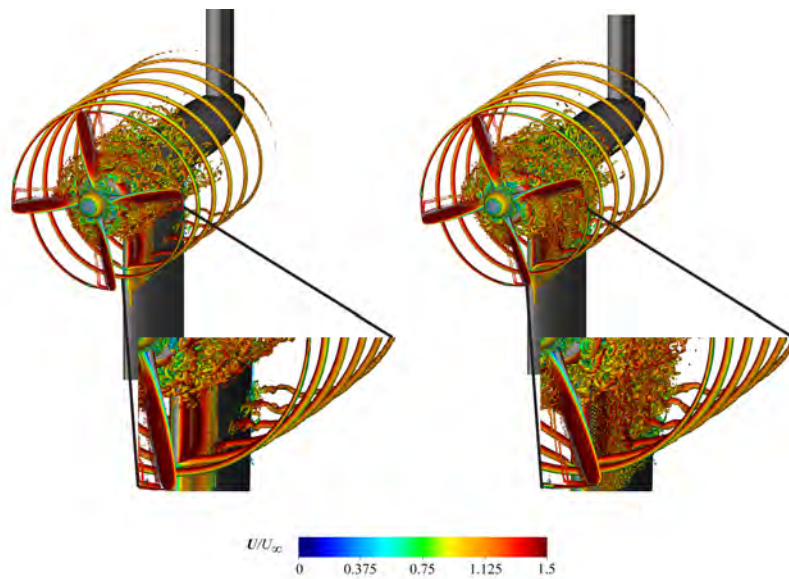


Figure 13: Instantaneous flow visualisation of the impingement of a propeller slipstream with on a pylon with solid (left) and permeable (right) leading edge

²¹¹ *Written by F. Avallone (f.avallone@tudelft.nl), D. Ragni, D. Casalino, Delft University of Technology, The Netherlands.*
²¹²

214 **3. Fan and Jet Noise**

215 *3.1. Aerodynamic noise of large-scale vortex ring produced by explosion*

216 Aeroacoustic properties of large-scale turbulent vortex rings produced by means of explosion
217 in steel cylindrical chambers (Fig. 14) are considered [35]. Unlike the small-scale experiments
218 in which the noise of the ring is determined by spectra averaging over an ensemble of similar
219 realizations, in the case of large-scale rings generated by the explosion it is possible to investigate
220 the phenomenon on the basis of only a single realization. It significantly extends the range of
221 parameters that can be analyzed. The large-scale ring noise manifests itself by strong peaking
222 of the spectrum in a narrow frequency band as well as the small-scale one (Fig. 15). However
223 one could recognize two or even three narrow frequency bands which are close to the multiple
224 frequencies of the main peak (Fig. 16), but the amplitudes of these peaks are significantly lower.
225 The main frequency peak does not shift to a lower-frequency region while the ring moves. It
226 fundamentally differs from the case of the small-scale rings, which in turn is in agreement with
227 the self-similar theory of the vortex ring motion [36]. This difference means that the vortex
228 core behavior of such vortices has some peculiarities, although the presence of several peaks is
229 consistent with the results of the theory of vortex ring sound generation [37].



Figure 14: High speed camera diagnostics of vertical movement of the vortex ring, duct diameter 80 cm.

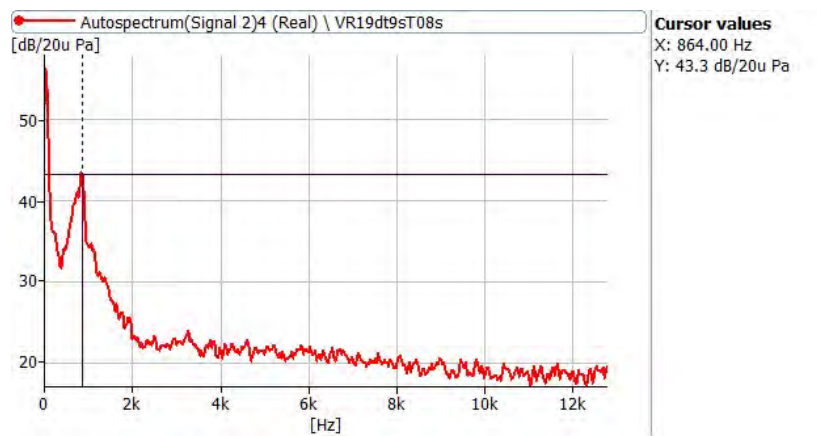


Figure 15: Narrow band spectra for the vortex ring with time delay after explosion 10 s, duct 80 cm.

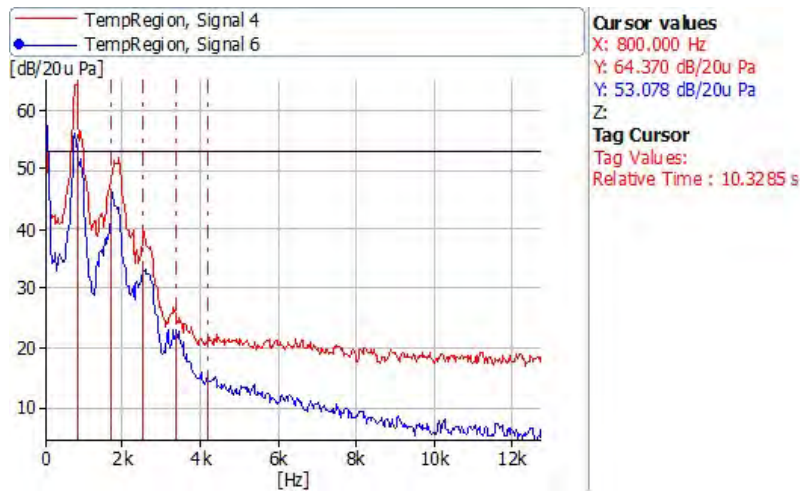


Figure 16: Multi-peaking structure of vortex ring noise for different conditions. Vortex ring moves along the ground surface, measurements produced by two different mics located at different distances from the trajectory (different colors).

230 *Written by V.F.Kopiev: (vkopiev@mksagi.ru), TsAGI, Russian Federation.*

231 **Submission Country: Russian Federation**

232 *3.2. Shockwave Generation and Radiation from an UHBR Engine with Flow Distortion using a*
 233 *CFD/CAA Chaining Strategy*

234 In the framework of the Clean Sky2 ASPIRE project, aeroacoustic investigations were
 235 achieved on a full-scale Ultra High Bypass Ratio (UHBR) engine with inflow distortion at tran-
 236 sonic conditions [38]. Computational Fluid Dynamics (CFD) simulations were first realized to
 237 compute the shocks in the vicinity of the fan, which were then radiated outside of the nacelle
 238 thanks to Computational AeroAcoustics (CAA) simulations. The elsA solver [39] was used for
 239 both CFD and CAA simulations and the coupling was done by injecting the shocks in terms of
 240 usual conservative variables using a non-reflecting boundary condition [40]. The CAA solver
 241 is based on the non-linearized Euler equations which allows to define the CFD/CAA interface
 242 close to the fan where the propagation of shocks is highly non-linear. Both shock generation
 243 and shock propagation mechanisms were investigated and the effects of inflow distortion were
 244 highlighted by comparison with a baseline case without distortion. It was shown that the distor-
 245 tion, characterized by an acceleration of the flow at the bottom of the nacelle (17), is responsible
 246 for a modification of the shock amplitudes that depends on the circumferential position. Thus,
 247 azimuthal modes appear in addition to the rotor-locked mode present without distortion. The
 248 near-field radiation is highly impacted with most of the noise being directed towards the sky
 249 (18). This is shown to be caused by the blockage of shocks by a supersonic flow region in the
 250 bottom of the nacelle (19). ONERA carried out this study in close cooperation with partners
 251 Airbus, NLR, and DLR and received funding from the Clean Sky 2 Joint Undertaking under the
 252 European Unions H2020 program (grant agreement no. 681856).

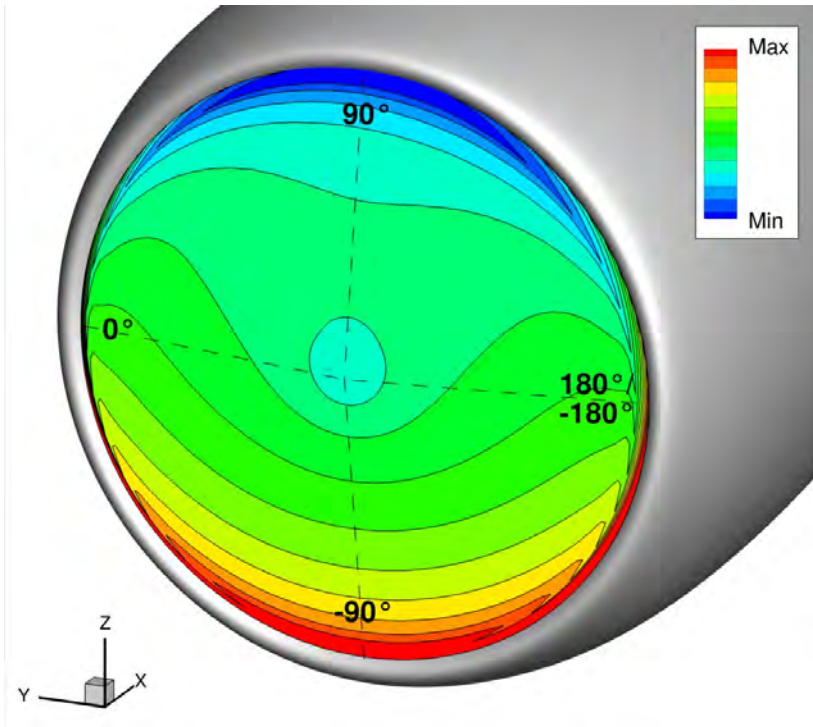


Figure 17: Inflow distortion map (axial velocity contours).

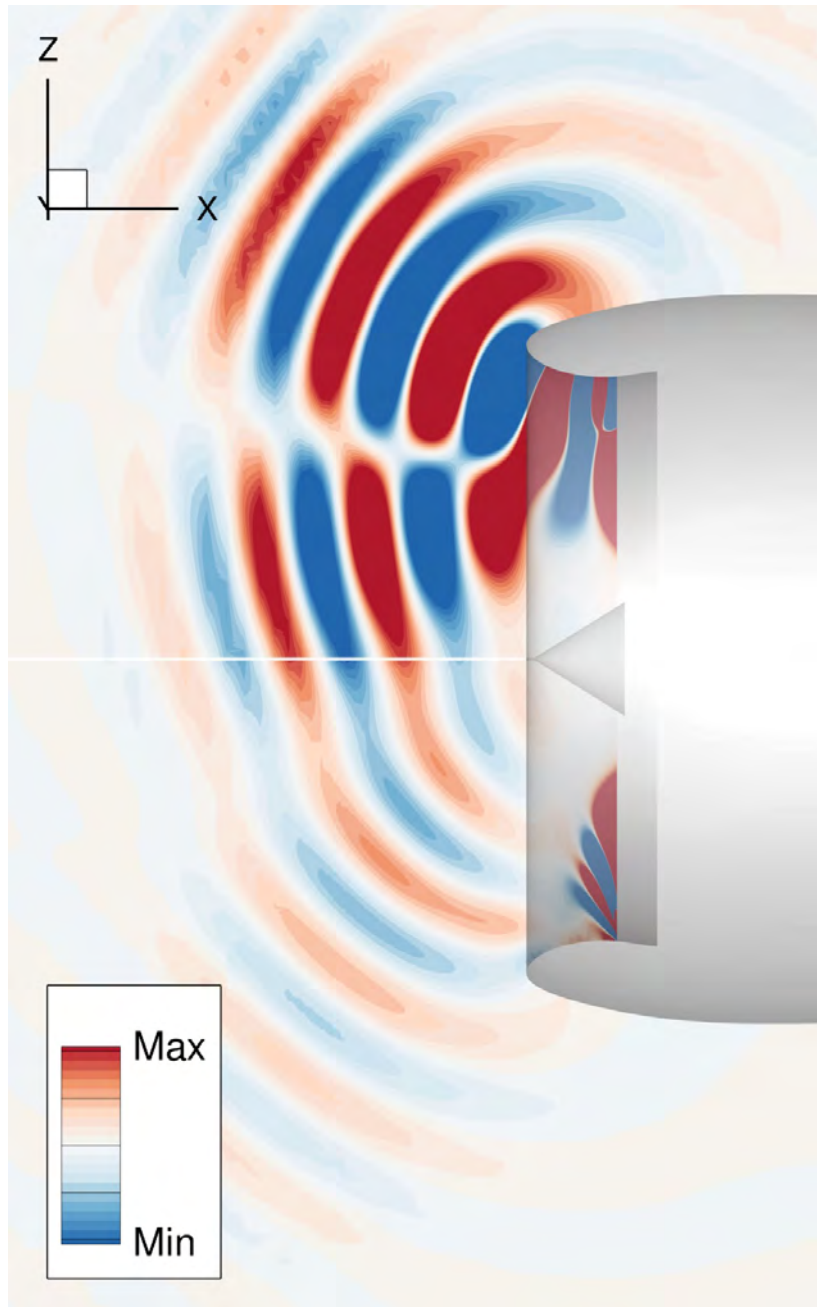


Figure 18: Pressure radiated through the inlet at the BPF (vertical plane).

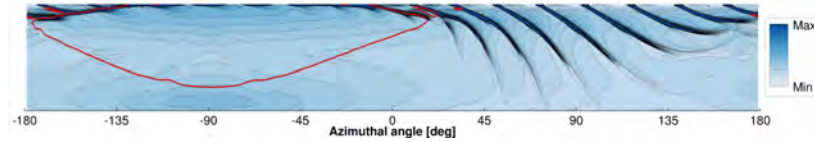


Figure 19: Instantaneous density gradient magnitude contours and sonic isoline (in red) in the inlet (unwrapped radial slice, the fan is at the top, the nacelle entrance is at the bottom).

253 *Written by M. Daroukh: majd.daroukh@onera.fr, C. Polacsek, A. Chelius, ONERA - The French*
 254 *Aerospace Lab, Châtillon, France.*

255 **Submission Country: France**

256 *3.3. A novel facility for the investigation of fan noise generation mechanisms: ECL-B3*

257 The fan module is expected to be the major noise source of future Ultra-High-Bypass-Ratio
 258 (UHBR) turbofan engines. Among the reasons are the increase in fan diameter, a reduction of
 259 the exhaust jet speed and the shortening of the nacelle. The new ECL-B3 test rig shown in Fig 20
 260 is dedicated to advanced research in aeroacoustics [41] as well as aero-dynamic and aero-elastic
 261 instabilities of fan stages [42]. This facility, the result of a collaboration between the Fluid Me-
 262 chanics and Acoustics Laboratory and Safran Aircraft Engines, was inaugurated in 2018 at the
 263 Ecole Centrale de Lyon. The first tested configuration was a scaled modern UHBR fan manu-
 264 factured by Safran Aircraft Engines within the ENOVAL European project. The noise generated
 265 by the fan module was measured by in-duct wall-flush mounted microphones intended for the
 266 characterization of the modal content. Part of the sensors are mounted on rotating rings allow-
 267 ing a fine spatial discretization. The angular steps have been optimized such as to minimize
 268 the number of rotating steps while keeping modal basis parameters such as the mutual coher-
 269 ence and condition number as low as possible over a wide frequency band. The invariably lost
 270 phase relationships between probes at the sequential positions is reconstructed. fixed reference
 271 microphones have been used to estimate the complete cross-spectral matrix as if measurements
 272 at sequential steps were recorded simultaneously. Modal amplitudes are estimated by using an
 273 iterative Inverse Bayesian Approach [43]. The resulting algorithm allows to control the degree
 274 of sparsity imposed on the solution. For instance at tonal frequencies the number of dominant
 275 modes is expected to be small due to constructive interferences, a high degree of sparsity is
 276 appropriate. For broadband noise a mild sparsity assumption would be more pertinent [41].

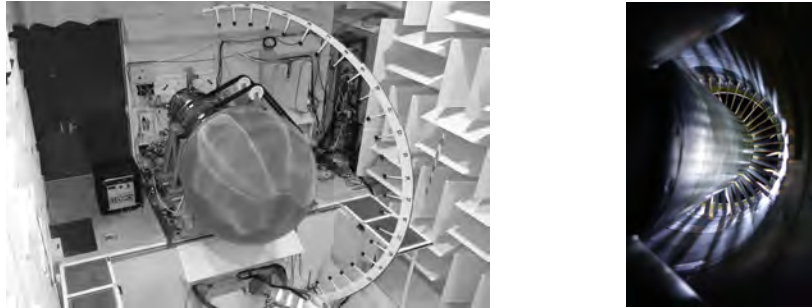


Figure 20: Left, view of the Turbulence Control Screen (TCS) and the traversable microphone array for directivity measurements in the anechoic chamber of the ECL-B3 facility. Right, in-duct view from the downstream test section showing stator vanes.

277 *Written by Antonio Pereira: antonio.pereira@ec-lyon.fr, Laboratoire de Mécanique des Fluides*
278 *et d'Acoustique, Ecole Centrale de Lyon, France, Mathieu Gruber, Safran Aircraft Engines,*
279 *France.*

280 **Submission Country: France**

281 3.4. Multi-port eduction of installation effects applied to a small axial fan

282 In HVAC systems, the noise emitted by the fan is usually characterized in a test bench ensur-
283 ing a relatively ideal constant and uniform inflow. In contrast, the implementation of this fan
284 in an industrial duct system will often result in a non-uniform and unsteady flow field due to
285 the presence of nearby bends, valves, etc. Those distorted inflow conditions are usually accom-
286 panied by an increase of noise emissions [44]. An experimental investigation of aeroacoustic
287 installation effects was performed in the ALCOVES (Aeroacoustic Lab for COoling and VENTI-
288 lation Systems) test bench of the von Karman Institute for Fluid Dynamics [45] for the case of an
289 axial fan such as found in domestic appliances. A multi-port methodology [46] has been used to
290 extract the active noise emitted by the fan in various inflow conditions, by decontaminating the
291 microphone measurements from the test bench acoustic reflections and turbulent boundary layer
292 pressure fluctuations. The inflow distortions were shown to have strong impact on the acoustic
293 emissions and aerodynamic performance of the fan. Using similarity laws, it was shown that
294 the alteration of the operating point is not sufficient to explain the impact of distorted inflows on
295 the acoustic power radiated by the fan. The broadband noise in particular was shown to be very
296 sensitive to the turbulence shed by the grids, with additional noise of the order of 10 dB at some
297 frequencies in Fig. 21. The results suggest the need for novel acoustic design guidelines ac-
298 counting for inflow quality in addition to the classical indicators solely based on the performance
299 point.

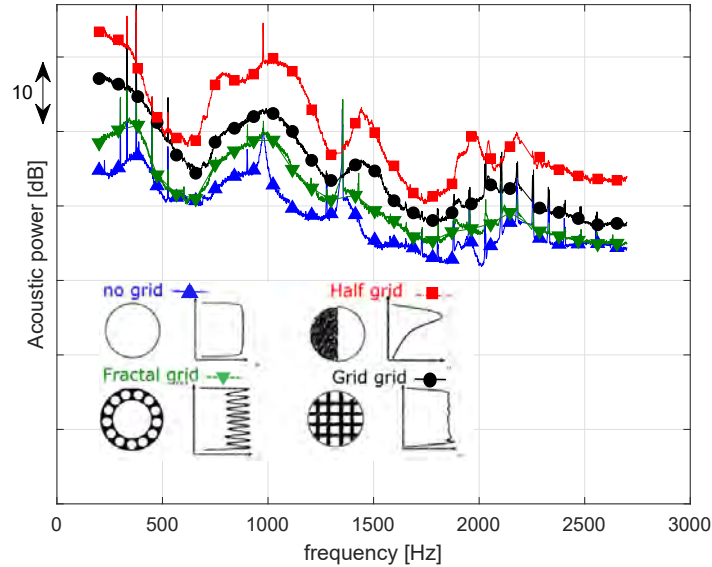


Figure 21: Acoustic power upstream of the fan under different inflow conditions at the same rotational speed.

300 *Written* *Written* *by* *Joachim* *Dominique* *(* *Joachim.dominique@vki.ac.be**)*, *Christophe*
 301 *Schram*, *Julien* *Christophe*, *von* *Karman* *Institute*, *Belgium* *and* *Raul* *Corralejo*
 302 *(raul.corralejo@dyson.com)*, *Dyson* *Ltd*, *Malmesbury*, *England*.

303 **Submission Country: Belgium**

304 *3.5. Prediction of far-field sound of installed complex geometry ultra high bypass ratio jets in*
 305 *flight using LES*

306 Growing aero-engine bypass ratios means the noise directly generated by the jet has now de-
 307 creased significantly. Another consequence is that the relative importance of installation noise
 308 has increased. Increasing engine diameters can lead the jet to directly interact with the wing
 309 and flap generating significant noise sources. Using LES in a blind test, flow and resulting far-
 310 field sound has been accurately predicted for complex geometry installed configurations under
 311 flight conditions [47]. This is difficult and costly to adequately achieve experimentally, yet well
 312 defined numerically. Figure 22 shows the jet-wing-flap interaction and far-field sound directly
 313 below the aircraft. Agreement with available measured sound data is clear. Isolated and installed
 314 configurations, have been contrasted for round nozzles with two flap deflections [47] and noz-
 315 zles with serrations [48]. For round nozzles a 20dB increase in noise was predicted and greatly
 316 reduced with nozzle serrations. This is due to increased turbulence dissipation reducing jet-flap
 317 interaction. Using high-fidelity unsteady data sets, noise sources and their distribution have been
 318 identified [47]. Furthermore, turbulence length and time scale distributions have been calculated
 319 [47, 49] to inform lower fidelity modelling such as RANS, that can be used to guide rapid design
 320 tools. A modelling framework has been defined for complex geometries [47] consisting of mod-
 321 ular hybrid structured-unstructured mesh generation, low dissipation numerical discretisation,

322 hybrid LES-RANS turbulence modelling, Ffowcs Williams-Hawkings (FW-H) surface genera-
 323 tion and far-field propagation [47]. The same procedure has recently been successfully validated
 324 in another blind test for large scale simulations including a pylon and fuselage. This highlights
 325 the ability of the approach to reliably replace significant amounts of rig testing, also providing
 326 greater consistency.

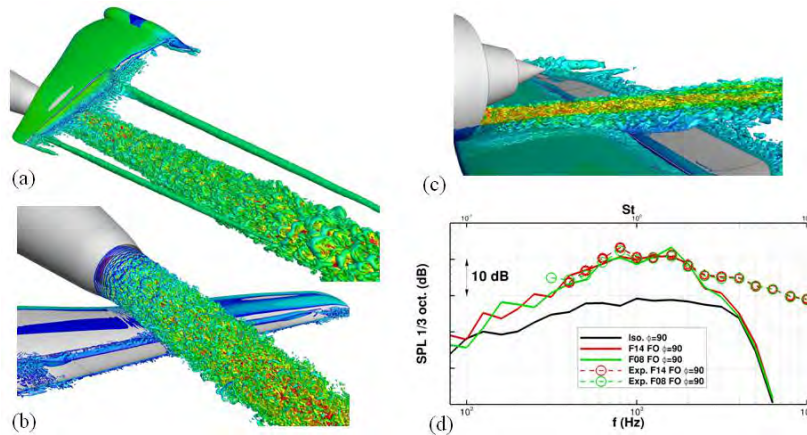


Figure 22: Fig. 1 (a-c) Jet flow and interaction with wing-flap geometry, (d) isolated (Iso.) and installed sound pressure level for flap deflections 8 (F08) and 14 (F14) degrees with measured (Exp.) data.

327 *Written by J. C. Tyacke: james.tyacke@brunel.ac.uk, while at the Department of Engineering,*
 328 *University of Cambridge, UK*

329 **Submission Country: UK**

330 4. Helicopter Noise

331 4.1. Blade-Vortex Interaction Noise Controller Based on Miniature Trailing Edge Effectors

332 A methodology to suppress/alleviate the noise annoyance emitted by bladevortex interaction
 333 (BVI) phenomena occurring on helicopter main rotors developed and validated in Refs. [50, 51]
 334 has been presented. The proposed methodology is suitable for the identification of multi-cyclic
 335 harmonic controllers based on the actuation of rotor blades equipped with Miniature Trailing
 336 Edge Effectors (MiTEs). The low-power requirements make MiTEs particularly suited for this
 337 kind of application. The objective of the control methodology is the direct suppression of the
 338 aerodynamic noise sources by generation of localized high-harmonic unsteady aerodynamic
 339 loads (as much as possible equal and opposite to those produced by BVI phenomena) aimed
 340 at canceling out those caused by the BVI events. The set-up of control devices is selected on
 341 the basis of the blade-vortex interaction scenario, taking into account a trade-off between effec-
 342 tiveness and power requirement. The control law is efficiently identified by means of an optimal
 343 controller synthesized through suitable two-dimensional multi-vortex, parallel blade-vortex in-
 344 teraction problems. The proposed methodology is validated by the application to realistic heli-
 345 copter main rotors during low-speed descent flights, numerically simulated through high-fidelity
 346 aerodynamic and aeroacoustic solvers based, respectively, upon a three-dimensional free-wake

347 boundary element method [52] for the solution of potential flows around rotors in blade-vortex
348 interaction conditions and the Farassat 1A formulation. Results demonstrate that the proposed
349 control approach is a promising method to reduce BVI noise.

350 *Written by S. Modini (saramodini@gmail.com), G. Graziani, University of Rome Sapienza, Italy*
351 *and M. Gennaretti, G. Bernardini, Roma Tre University, Italy).*

352 **Submission Country: Italy**

353 4.2. Rotorcraft comprehensive code assessment for blade-vortex interaction conditions

354 Computational methodologies applied to a comprehensive code for rotorcraft developed in re-
355 cent years at Roma Tre University are presented in Ref. [52], along with an assessment of its
356 prediction capabilities focused on flight conditions characterized by strong blade-vortex interac-
357 tion phenomena. This comprehensive code includes a detailed aeroelastic response analysis of
358 the blade within the trim procedure: a three-dimensional, potential-flow, an rotor aerodynamics
359 solver which is fully coupled with a bending-torsion beam model of blade structural dynamics,
360 and a harmonic-balance/modal approach is used to integrate the rotor aeroelastic equations [53].
361 Hence, for a prescribed flight condition, the aeroelastic trim module provides pitch control set-
362 tings and vehicle attitude, blade elastic response, mean and vibratory hub loads, as well as the
363 pressure distributions required to define the noise sources in the aeroacoustic module. The rotor
364 noise radiation is evaluated through the widely-used boundary integral Farassat 1A formulation.
365 The validation campaign of the comprehensive code has been carried out against the well-known
366 HART II database, which is the outcome of a joint multi-national effort aimed at performing wind
367 tunnel measurements of loads, blade deflection, wake shape and noise concerning a four-bladed
368 model rotor in low-speed descent flight. Comparisons with numerical simulations available in the
369 literature for the same test cases are also presented. It is shown that, with limited computational
370 cost, the results provided by the Roma Tre aero-acousto-elastic solver are in good agreement with
371 the experimental data, with a level of accuracy that is in line with the state-of-the-art predictions.
372 The influence of the vortex core modeling on aerodynamic predictions and the influence of the
373 inclusion of the fuselage shielding effect on aeroacoustic predictions are discussed.

374 *Written by M. Gennaretti: massimo.gennaretti@uniroma3.it, G. Bernardini, J. Serafini, Univer-*
375 *sity ROMA TRE, Italy and G. Romani, Delft University of Technology, The Netherlands*

376 **Submission Country: Italy**

377 5. Aircraft interior noise

378 5.1. Parametric study on effects of wall pressure wavenumber spectra on aircraft fuselage vibra- 379 tion

380 The wall pressure wavenumber spectra in the front region of the aircraft fuselage at cruise
381 condition are formulated based on the wall pressure cross-spectral model [54]. The formulated
382 spectra are used as excitation sources for the calculation of the fuselage panel vibration with
383 the Statistical Energy Analysis method [55]. The coherence length, the convection velocity and
384 the flow angle are modified to study their effects on the wavenumber spectrum and the panel
385 vibration. Furthermore, the practical impact of parametrically important factors on the calculated
386 results such as the surface microphone array size and resolution, window functions and dealing
387 with noisy signal is studied, see [56]. Figs. 23 and 24 show the effect of coherence length

388 and convection velocity modifications on the wavenumber spectra and the panel vibration. For
 389 the frequencies between 800 Hz and 2 kHz in which a possible coincidence between the flow
 390 excitation and the panel vibration occurs, the wavenumber spectral peak region is important
 391 for the excitation. A change in the spectral peak level results in a respective change in panel
 392 vibration level. For frequencies outside of 800 Hz – 2 kHz, the lower streamwise wavenumber
 393 spectral range is important for the excitation. Figs. 25 and 26 show the effect of the array size,
 394 resolution and noise. A too small resolution or a too small size will strongly affect the calculated
 395 wavenumber spectra and vibration. However, an overly large array size will increase the error
 396 due to a reduction of the signal-to-noise ratio when dealing with noisy signal.

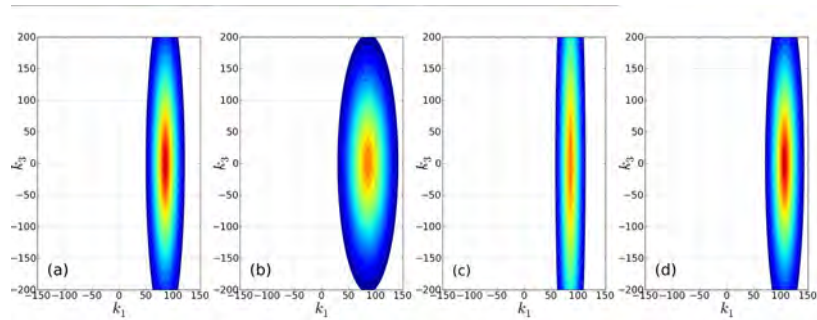


Figure 23: Contour plot of wavenumber spectra at 2500 Hz with levels between -54 dB and -35 dB (a) Smol'yakov model (b) $0.5 l_1$ (c) $0.5 l_3$ (d) $0.8 u_c$

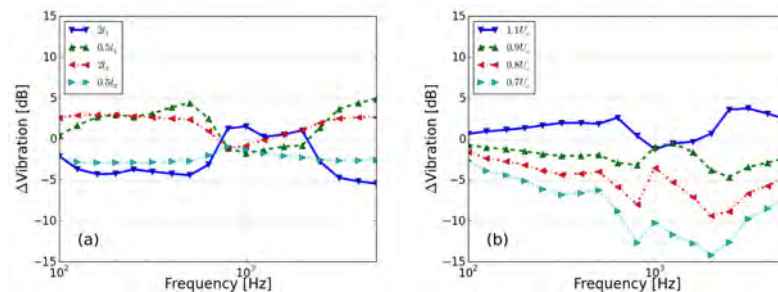


Figure 24: Comparison of panel vibration (a) modification of coherence lengths (b) modification of convection velocities.

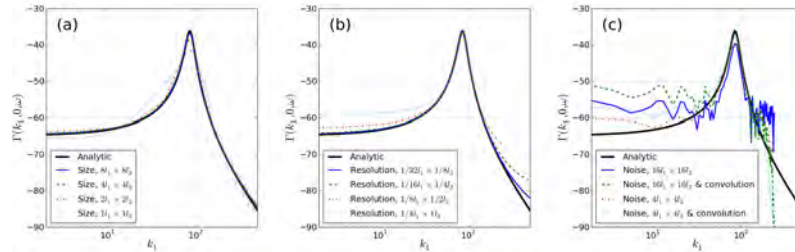


Figure 25: Comparison of streamwise wavenumber spectra at 2500Hz with different processing settings (a) array sizes (b) array resolutions (c) noisy signal.

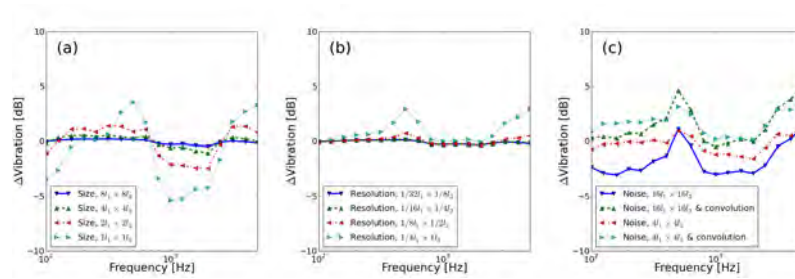


Figure 26: Comparison of panel vibration with different processing settings (a) array sizes (b) array resolutions (c) noisy signal.

397 *Written by Nan Hu: nan.hu@dlr.de, DLR, Germany, Sören Callsen, Airbus Operations GmbH,*
 398 *Germany*
 399 **Submission Country: Germany**

400 6. Propeller noise

401 6.1. Contra-rotating open rotors (CROR) as a viable aircraft propulsion system: experimental, 402 numerical and analytical studies.

403 Noise from contra-rotating open rotors is a major obstacle to the adoption of this fuel efficient
 404 technology as a viable aircraft propulsion system. A better understanding of both contra-rotating
 405 open rotor noise generation, reduction and shielding has been achieved recently due to ongoing
 406 research based on the WENEMOR data [57, 58, 59] where 288 test conditions of a 1:7 scale
 407 green regional aircraft model were completed. A wide range of airframe configurations equipped
 408 with two installed CROR engines operating in both pusher and tractor modes and operated at
 409 both approach and takeoff settings were assessed as a function of windtunnel speed and angle
 410 of attack. The geometric parameters which were varied included interchangeable tailpieces (T,
 411 L and U empennage), variable fuselage length, engine pylon rotation, and engine pylon elonga-
 412 tion and these allowed shielding effects, pylon wake effects as well as the benefits to be gained
 413 from moving the entire CROR out of the wing wake to be assessed [60]. In addition to the full
 414 installation analysis set-up, a second campaign was conducted where only the installed-on-pylon

415 contra-rotating open rotor configuration was evaluated [61]. The experimental results were used
416 to validate an original numerical method for the calculation of engine noise installation effects
417 and its application to contra-rotating open rotor propulsion was demonstrated. This method is
418 based on the weak coupling between computational fluid dynamics, an integral method based on
419 Lighthills analogy for the calculation of acoustic radiation, and on a boundary element method
420 for the calculation of the acoustic diffraction by the aircraft fuselage and empennage [62, 63]. In
421 addition, the equal number of blades fore and aft for the CROR engines considered, has provided
422 interesting opportunities such as a study which approaches the question of counter-rotating open
423 rotor engine noise levels from a yet unexplored perspective, examining the radiation efficiency
424 properties of unducted turbomachinery acoustic modes in order to provide design guidelines that
425 mitigate the radiation of sound without the need for shielding [64].

426 *Written by John Kennedy: kennedj@tcd.ie, Trinity College Dublin, the University of Dublin.*
427 *Ireland*

428 **Submission Country: Ireland**

429 **7. Techniques and methods in aeroacoustics**

430 *7.1. The conditions of quadrupole moment conservation in the evolution of small perturbations* 431 *of stationary flows*

432 Perturbations of incompressible ideal fluid flows are described in terms of the Lagrangian
433 and Hamiltonian formalism [65]. Expressions for the Lagrangian and Hamiltonian in which
434 the displacement field and momentum density perturbation field are used as canonical variables
435 are obtained. Based on Noethers theorem, the conditions of conservation of the quadrupole
436 moment of perturbations of the flow are derived. It is shown that these conditions are satisfied
437 for any uniform jet flows both in the two- and three-dimensional cases. The results are of great
438 importance in aeroacoustics because the quadrupole moment of the flow is the principal term of
439 acoustic source expansion in the Mach number. Conservation of the quadrupole moment means
440 that the evolution of perturbations of uniform jet flows under arbitrary initial conditions makes
441 no contribution to quadrupole sound radiation in the linear approximation. Therefore, sound
442 sources of low-velocity jets may be related to finer effects, such as weak non-uniformity of the
443 flow in the streamwise direction or nonlinearity of perturbations. It is also possible that the idea
444 that sound sources in a turbulent jet are small perturbations on the background of the mean flow
445 does not correspond to their real nature and generation of acoustic perturbations in the turbulent
446 flow is significantly affected by the local non-linear structure of the vorticity.

447 *Written by Sergey Chernyshev and V.F. Kopiev (vkopiev@mktsagi.ru), TsAGI, Russian Federa-*
448 *tion.*

449 **Submission Country: Russian Federation**

450 *7.2. Noise reduction of VEGA launch pad environment at lift-off*

451 In 2015, ONERA performed the analysis of microphone array data measured during VV05 of
452 VEGA launcher in Kourou, on behalf of ESA [66]. Approximately at the payload fairing level, a
453 2 m diameter circular array composed of 32 microphones, was implemented on one of the anti-
454 lightning pylons, oriented toward the exhaust duct, aimed at identifying the location and level of
455 the acoustic sources generated during lift-off. Based on this study, the contributions to the overall

456 noise from the engine jet, the table and the flame trenches were highlighted and as a trade-off
 457 between acoustic benefits and costs, ESA decided to modify the launch table by closing existing
 458 openings with heavy steel plates filled with porous materials. Two years later, in 2017, during
 459 VV10, the same microphone array measurements were realized. Direct comparison of the acoustic
 460 levels measured on the microphones pointed out a reduction of about 2 dB at the frequencies
 461 of interest, and even more for higher frequencies. A deconvolution method developed in ONERA
 462 [67], based on the well-known DAMAS [68], was applied to three scanning plans, including a total
 463 of about 3000 sources. When the launcher is at the lowest altitudes, corresponding to the most
 464 critical moment for acoustics, the source localization confirmed strong reduction of the sources
 465 radiated from the table, with only slight change from the flame trenches (Fig 27). The last step
 466 consisted in propagating the acoustic sources to the fairing. As the microphone array is in front
 467 of one of the two ducts, the reasonable hypothesis that they generate similar noise (uncorrelated)
 468 is made and the sources identified on the flame trench are symmetrized. Diffraction effect on
 469 the fairing is taken into account thanks to correction of infinite cylinder. The results (Fig 28) are
 470 coherent: the effect of the table covers progressively decreases with the increasing distance of
 471 the launcher from the pad, leading to a corresponding reduction of the acoustic benefit.

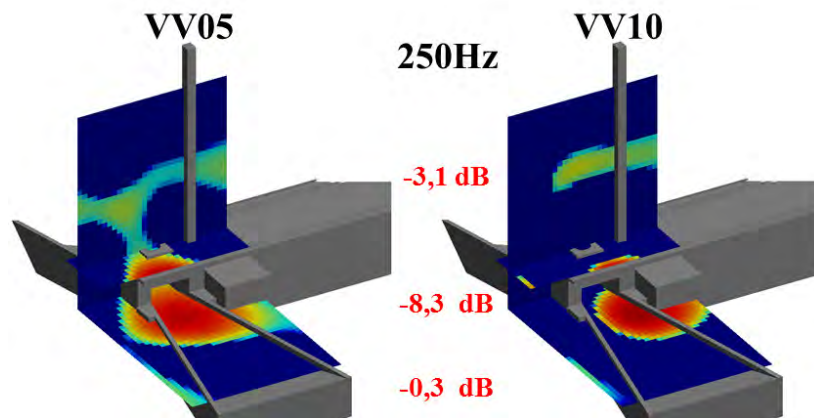


Figure 27: Acoustic reduction on each scanning plan at 0 m

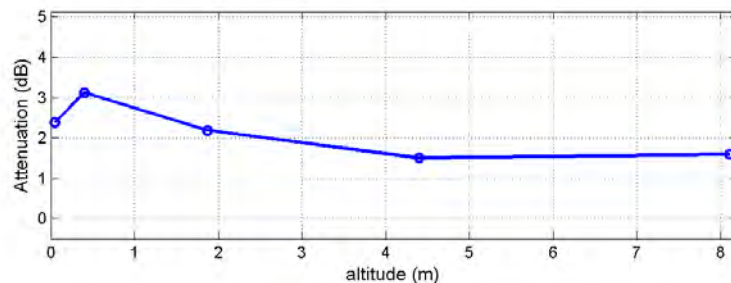


Figure 28: Acoustic attenuation at the fairing level Evolution with the altitude

472 Written by F. Cléro: *franck.clero@onera.fr*; F. Mortain, ONERA, France, D. Palmieri, ESA-
 473 ESRIN, Italy

474 **Submission Country: France**

475 *7.3. Duct azimuthal and radial modal deconvolution of CFD analysis of UHBR engine tonal*
 476 *noise.*

477 A modal deconvolution method is used to characterize the main propagating acoustic duct
 478 modes from non-intrusive measurements. In the framework of the ASPIRE-CS2 project, ON-
 479 ERAs modal deconvolution method ARMADA [69] is applied to numerical data from a generic
 480 UHBR engine at the take-off sideline condition. The numerical simulation is provided by NLR
 481 to quantify the tonal internal acoustic field by the application of a CFD approach for the config-
 482 uration with a clean fan channel [70]. The complex geometry of the nacelle implies a variable
 483 Mach number through the fan duct, which is unfortunately not precisely known. As a first step,
 484 an azimuthal Fourier transform is applied to determine the content of the dominant azimuthal
 485 modes. In the bypass duct (downstream direction), they are shown to be quite constant, whereas,
 486 upstream from the fan, they vary significantly in the vicinity of the inlet. Therefore, our decon-
 487 volution method [69], extended to an annular duct, is only applied on the bypass duct, using
 488 data obtained at BPF2 on the wall as it would be for flush mounted microphones. We consider
 489 a modal basis restricted to azimuthal mode orders from -1 to 11, which is relevant to explain the
 490 main content of the total sound pressure. Considering a constant flow rate with two hypotheses
 491 of Mach number (0.4 and 0.5), and under the correlated mode assumption, the results explain
 492 more than 74% of the data. The more energetic modes correspond to azimuthal mode $m=4$ and
 493 radial modes $n=2$ and 3, together with $m=3$ and $n=2$; they are found to be perfectly correlated.
 494 Modes propagating in the upstream direction (k^-) point out possible reflections at the end of the
 495 nacelle (see Fig. 29).

496 Finally, the acoustic pressure field (absolute value of the Fourier transform) is reconstructed
 497 from the estimated modes (cross spectral matrix of the amplitude), and compared to the initial
 498 numerical data (see Fig. 30). The black frames highlight areas where some modes, not included
 499 in the modal basis, go from cut-on to cut-off. Using only data obtained on the wall, ONERAs
 500 deconvolution method succeeds in providing a good representation of the acoustic field in the
 501 bypass duct.

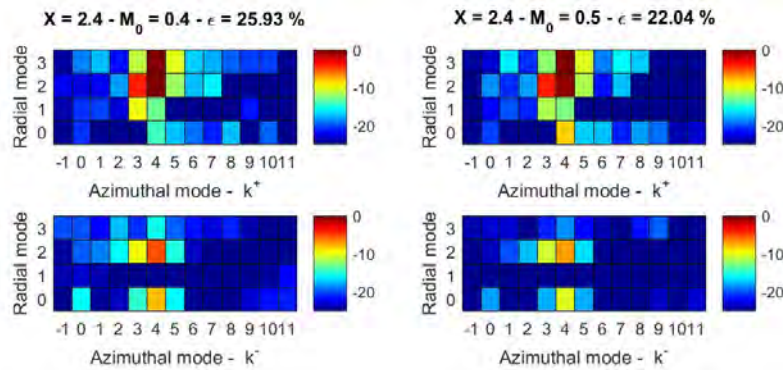


Figure 29: Normalized power cross spectral matrix of the amplitude of the modes obtained by correlated ARMADA on the bypass duct @BPF2, considering $M_0=0.4$ (left) and $M_0=0.5$ (right).

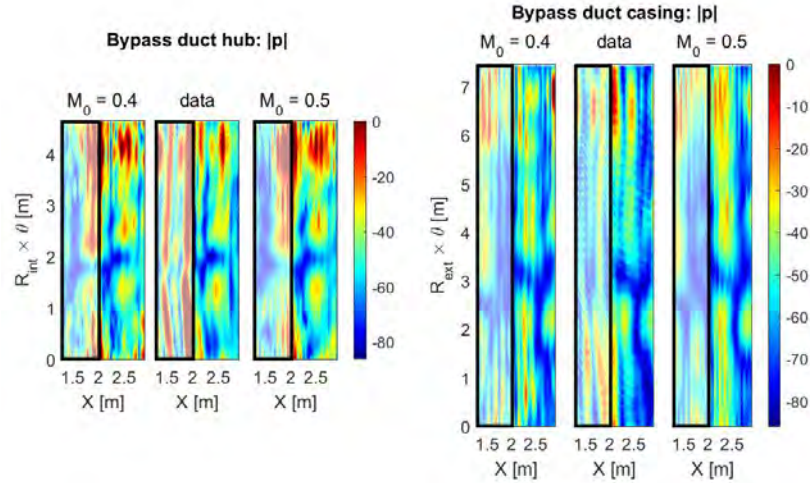


Figure 30: Absolute value of the Fourier transform of the pressure field reconstructed on the bypass duct hub surface (left) and duct casing surface (right).

502 *Written by S. Fauqueux: Sandrine.Fauqueux@onera.fr, French Aerospace Lab (ONERA), Aero-*
 503 *dynamics Aeroelasticity Acoustics Department, Châtillon, France*

504 **Submission Country: France**

505 *7.4. Uncertainty quantification for direct aeroacoustics of cavity noise*

506 Cavity noise has become a major concern in automobile exterior aerodynamics. Different
 507 noise generation mechanisms have been identified, such as Helmholtz resonance, standing waves
 508 and Rossiter feedback, which all lead to tonal noise emission. Both frequencies and sound pres-
 509 sure levels of cavity noise are highly sensitive to geometric and environmental uncertainties.
 510 Those sensitivities can lead to deviating results between experiment and numerical simulations.
 511 Uncertainty quantification (UQ) is therefore a promising tool to gain deeper insight into the fac-
 512 tors influencing the sound spectra. An UQ framework based on the deterministic high-order
 513 discontinuous Galerkin solver FLEXI has been developed to quantify the influence of random
 514 input parameters on cavity noise. UQ was realized through a non-intrusive spectral projection
 515 method which revealed fast stochastic convergence in comparison to sampling based methods.
 516 With the help of this framework, the system response of a cavity flow problem under the influence
 517 of uncertain parameters has been analyzed. Uncertainties in the upstream boundary layer as well
 518 as randomness in the cavity geometry have been investigated [71]. As an example, the acoustic
 519 response to an uncertain cavity depth revealed strong non-linearities. For a given critical cavity
 520 depth, sudden mode switching of the first two dominant Rossiter modes and the associated dis-
 521 tinct frequencies has been identified (Fig 31 left). The resulting pressure spectrum provided the
 522 stochastic noise production which included all dominant, unstable modes and can be interpreted
 523 as the superimposition of two distinct feedback regimes (Fig 31 right).

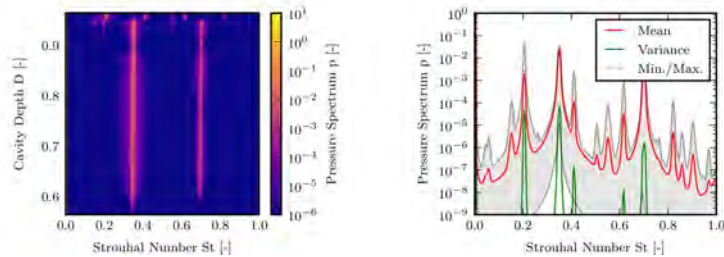


Figure 31: Influence of an uncertain cavity depth D on aeroacoustic feedback. Response surface plotted as a Campbell diagram (left). Stochastic pressure spectrum with expectation and variance (right).

524 *Written by Thomas Kuhn (thomas.kuhn@iag.uni-stuttgart.de), Daniel Kempf and Claus-Dieter*
 525 *Munz, Institute of Aerodynamics and Gas dynamics, University of Stuttgart, Germany*

526 **Submission Country: Germany**

527 *7.5. Simulating Tonal Fan Noise of an Aircraft in Flight*

528 To ensure compliance with noise regulations, expensive fly-over tests are needed. No numer-
 529 ical alternative currently exists. Yet an accurate virtual fly-over would revolutionize the design
 530 process of future aircraft as it can help to assess the most relevant noise sources at an early de-
 531 sign stage. As a first step towards enabling such a virtual fly-over, Mößner et al. [72] developed
 532 a method capable of studying tonal rotor-stator-interaction noise from its generation in the fan
 533 stage to its propagation to observer positions at ground level. Solving this problem with a single,
 534 high-fidelity method is hardly realizable, particularly in terms of computation costs. Instead,
 535 a computational chain consisting of multiple high-fidelity methods was established. The entire
 536 task was split into smaller subtasks that can be handled by specialized tools with the aim of
 537 performing each subtask as accurately and efficiently as possible. Different subtasks include the
 538 fan noise generation, the propagation in the bypass and inlet ducts and the shielding and scatter-
 539 ing effects due to the engines installation. Special care was taken to validate the accuracy of
 540 the interfaces between the tools. To ensure that the entire computational chain delivers plausi-
 541 ble results, the results were compared to another simulation [73] using an established technique
 542 for the case of an isolated engine and a good agreement was found. To prove the new methods
 543 capability of predicting the tonal fan noise of an installed engine, the technique was applied to
 544 a V2527 engine mounted underneath the fully equipped wing of an A320 aircraft in approach
 545 conditions (shown in Fig 32). In Fig 33, the acoustic footprint on the ground is shown for the
 546 isolated and installed engine cases. For the installed engine, scattering effects cause a complex
 547 interference pattern. The overall magnitude of sound pressure level and general directivity of the
 548 installed and isolated engine cases is, however, comparable for the investigated configuration. In
 549 summary, the efficiency of the method as well its capability for computing complex scattering
 550 effects was demonstrated. In future investigations, it is essential to incrementally increase the
 551 complexity of the simulation to pinpoint the most relevant noise mechanisms of fly-over tests.



Figure 32: Sound pressure of the isolated (left) and installed (right) engine cases

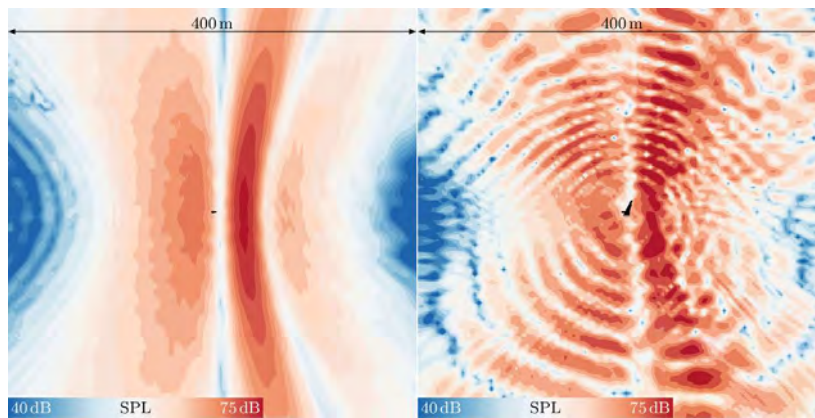


Figure 33: Acoustic footprint of the isolated (left) and installed (right) engine configurations

552 *Written by C. Kissner: carolin.kissner@dlr.de, M. Mößner, J. Delfs, L. Enghardt, German*
 553 *Aerospace Center (DLR), Germany.*

554 **Submission Country: Germany**

555 7.6. Enhanced HR-CLEAN-SC for resolving multiple closely-spaced sound sources

556 Enhancement of spatial resolution in acoustic imaging has been obtained by using an opti-
 557 mized acoustic array together with the Enhanced high-resolution (EHR) CLEAN-SC algorithm
 558 [74]. The EHR-CLEAN-SC algorithm is based on the well-known CLEAN-SC algorithm [75]
 559 that provides clean source maps in which sidelobes that are spatially coherent to the sources
 560 are eradicated. Still, the resolution of CLEAN-SC is limited by the Rayleigh criterion. The
 561 HR-CLEAN-SC algorithm [76] surpasses this limit, by explicitly accounting for the presence
 562 of closely-located sources. To find the locations of these sources, the source markers are re-
 563 located away from the peak in the source map, to a location where the combined influence of
 564 the other sound sources is minimal. The freedom of the source marker relocation is limited by
 565 the sidelobe level. A first step to enhance the HR-CLEAN-SC performance is to ensure low
 566 sidelobe levels by optimizing the array design. Secondly, the source marker relocation is done
 567 such that it exploits the low-sidelobe design of the acoustic array. It was demonstrated that the
 568 resulting EHR-CLEAN-SC algorithm could resolve four closely-spaced sound sources down to
 569 more than half the frequency set by the Rayleigh criterion, using both synthetic and experimental

570 data [74]. An example is shown in Fig. 34 presenting the source maps of four closely-spaced
 571 synthetic incoherent sound sources and using the standard Underbrink array. In subplots a to d,
 572 the results are shown for conventional frequency-domain beamforming (CFDBF), CLEAN-SC,
 573 HR-CLEAN-SC, and EHR-CLEAN-SC. Subplot e shows the results when the optimized array
 574 is used together with the EHR-CLEAN-SC algorithm. The maps are shown at a frequency of
 575 1.8 kHz, while, according to the Rayleigh criterion, the sources are expected to be resolved only
 576 above 4.2 kHz. In practice, the EHR-CLEAN-SC algorithm is recommended for examining
 577 closely-spaced aeroacoustic sound sources such as landing gear noise [77].

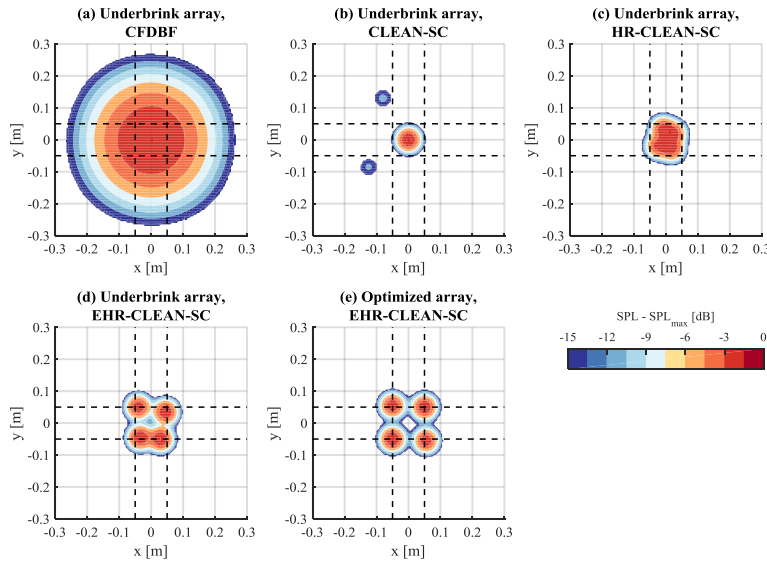


Figure 34: Source maps showing the sound pressure level relative to the maximum sound pressure level (SPL-SPL_{max}) of four synthesized sound sources with 10 cm separation produced by using the Underbrink array and (a) CFDBF, (b) CLEAN-SC, (c) HR-CLEAN-SC, and (d) EHR-CLEAN-SC, compared with the same source setting resolved by EHR-CLEAN-SC with the optimized acoustic array (e) at 1.8 kHz. (The sources are at the intersections of the dashed lines.

578 *Written by S.Luesutthiviboon: s.luesutthiviboon@tudelft.nl, A.M.N. Malgoezar, R. Merino-*
 579 *Martinez, M. Snellen, P. Sijtsma, D.G. Simons, Section Aircraft Noise & Climate Effects (ANCE),*
 580 *Faculty of Aerospace Engineering, Delft University of Technology, The Netherlands.*

581 **Submission Country: The Netherlands**

582 7.7. Statistical Inference Method for Liner Impedance Eduction with a Shear Grazing Flow

583 Understanding the effects of a complex flow on the acoustical response of nacelle liners is of
 584 prime importance for current nacelle liner design. The acoustical response of a liner is char-
 585 acterized by its impedance ζ , whose measurement, in the presence of a grazing flow, can be
 586 achieved through indirect eduction methods. These methods consist in matching an experimen-
 587 tal observation to a numerical simulation, via an optimization procedure. In practice, either the
 588 pressure field is measured on the wall opposite the liner [78], or the velocity field is observed

589 above the liner via a Laser Doppler Velocimetry (LDV) measurement [79], see Fig. 35. A set
 590 of equations (convected Helmholtz [78], linearized Euler [79]) is then chosen and solved numerically.
 591 The “numerical” pressure (or velocity) is then compared to its experimental counterpart
 592 until a convergence is reached. One of the main concerns regarding this strategy is the validity
 593 of the obtained impedance value, relative to the presence of different uncertainties. To take
 594 into account uncertainties of the measurements or the numerical model, the eduction is recast
 595 into a statistical inference problem. Using Bayes theorem, the posterior probability density of
 596 the impedance is obtained, thus representing the information one has on this quantity, after having
 597 observed new experimental data [80]. This approach allows taking into account different
 598 sources of uncertainties, available prior knowledge, and to yield estimators on the impedance
 599 that are more informative than the single impedance value returned by a classical deterministic
 600 approach. The statistical eduction process has been successfully validated on NASA benchmark
 601 data (from [78]). The results are shown in Fig. 36, for material CT57 (ceramic tubular material
 602 of 57% porosity), at Mach 0.255.

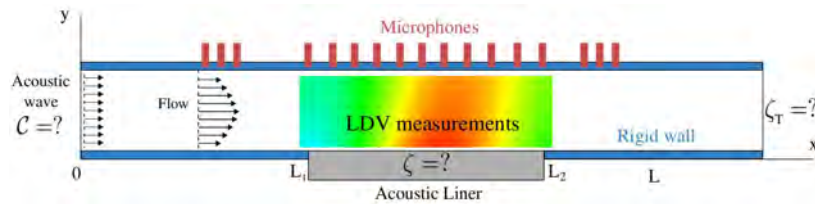


Figure 35: Schematics of an aero-acoustic bench for liner impedance eduction, showing both the microphone measurement locations and the LDV window.

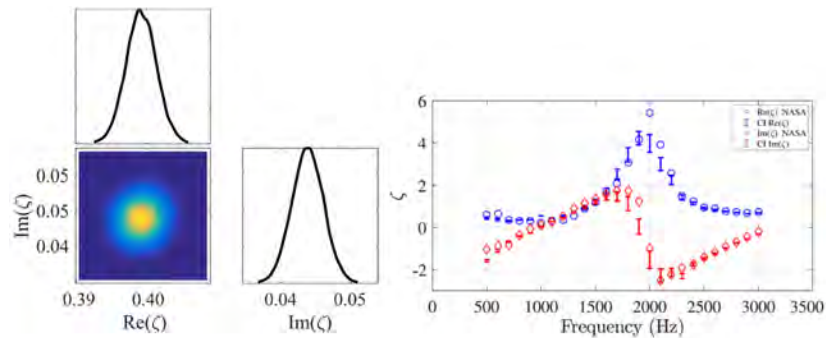


Figure 36: Left: probability density function of the impedance at $f = 1000$ Hz and Mach = 0.255. Right: comparison between NASA deterministic eduction method (markers) and Bayesian inference results (error bars), at Mach = 0.255

603 *Written by Rmi Roncen: remi.roncen@onera.fr; Fabien Mry, Estelle Piot and Frank Simon. ON-*
 604 *ERA, France*

605 **Submission Country: France**

606 7.8. Analysis and discretization of time-domain impedance boundary conditions in aeroacoustics
607

608 Improving the reliability of computational aeroacoustics (CAA) is one of the key drivers to
609 achieve the noise reduction levels targeted by international regulations. To reduce the noise emit-
610 ted by an aircraft, one practical solution consists in mounting passive sound absorbing materials,
611 commonly known as acoustical liners. Practical computations of sound absorption are typically
612 done by abstracting the geometrical features of the material using an impedance boundary condi-
613 tion, which in case of time-domain CAA simulations is called a TDIBC. The TDIBC used in the
614 numerical computation must be tailored to the absorbing material considered. [81] has shown
615 that the TDIBC can be derived from a mathematical study of the absorbing material, while being
616 shaped under an expression very close to an improved broadband multipole model. This fea-
617 ture contrasts with the existing purely empirical one-size-fits all approach (consisting in using
618 a single numerical model postulated a priori), which can lead to computational difficulties for
619 adjusting the fit. The analysis carried out has delivered tailored TDIBCs for a wide range of
620 materials, which covers perforates, semi-infinite ground layers, as well as cavities filled with a
621 porous medium. A computationally-efficient way of performing the time-domain computation
622 has also been laid out in [82]. It relies on using transport equations and ordinary differential
623 equations, and is also a consequence of the mathematical analysis used for tailoring the TDIBC.
624 Moreover, a practical problem encountered in numerical computations is that some materials can
625 impose a stringent reduction in time step, leading to a costly simulation. The analysis presented
626 in [82] has highlighted a way of canceling this time step reduction, i.e. of ensuring that the IBC
627 has a neutral impact on the simulation time step (see Fig. 37. This is done using a formulation
628 based on the reflection coefficient instead of the impedance or admittance.

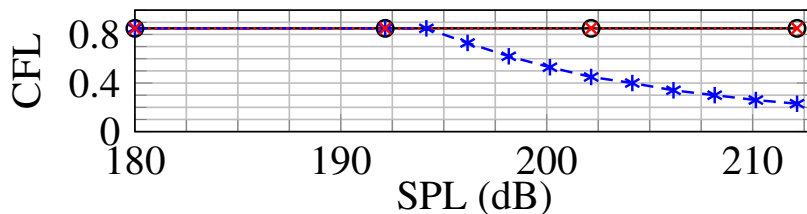


Figure 37: Maximum allowable CourantFriedrichsLewy (CFL) number against SPL, in an impedance tube configuration. Hard wall (black), non-linear TDIBC with a formulation based on the reflecton coefficient (red), non-linear TDIBC with a formulation based on the impedance (blue). The dB levels of the incident wave are arbitrary.

629 Written by E. Piot (*estelle.piot@onera.fr*), F. Monteghetti, ONERA, France, D. Matignon, ISAE-
630 Supaero, France.

631 **Submission Country: France**

632 7.9. Improved Generalized Inverse Beamforming for Airframe Noise Applications

633 Thanks to their ability to deal with distributed and coherent acoustic sources, inverse beam-
634 forming methods have grown in popularity amongst the aeroacoustic community in the last few
635 decades. An improved version of the Generalized Inverse Beamforming (GIBF) [83] has been
636 developed at von Karman Institute for Fluid Dynamics (VKI) with the objective of ensuring an

637 accurate source localization and a robust source strength reconstruction for airframe noise appli-
 638 cations. Specifically, a method based on the Quasi-optimality criterion for the determination of
 639 the optimal regularization parameters at each iteration of the algorithm has been implemented.
 640 The validation of the technique has been carried out by applying the improved GIBF to an ex-
 641 perimental benchmark dataset labelled as NASA2. The test case, Fig. 38, refers to the analysis
 642 of a small-scale open-jet facility, the NASA Langley Quiet Flow Facility (QFF), for the char-
 643 acterization of a NACA 63-215 Mod-B full-span airfoil self-noise. The study comprehends the
 644 qualitative evaluation of the noise source distribution maps for several one-third octave frequency
 645 bands and the quantitative estimation of the integrated one-third octave band spectra of the model
 646 leading edge and trailing edge regions. All the maps and the spectra have been compared with
 647 the ones obtained with other microphone phased array data processing techniques commonly
 648 used in aeroacoustic applications [84]. Results show that, with a proper handling of the regular-
 649 ization strategy, GIBF can accurately resolve distributed acoustic noise sources. The sound maps
 650 present improvements in terms of readability and reconstruction of the distributed nature of the
 651 source, whereas the integrated levels are in close agreement with the ones predicted by the other
 652 advanced methods Fig. 38.

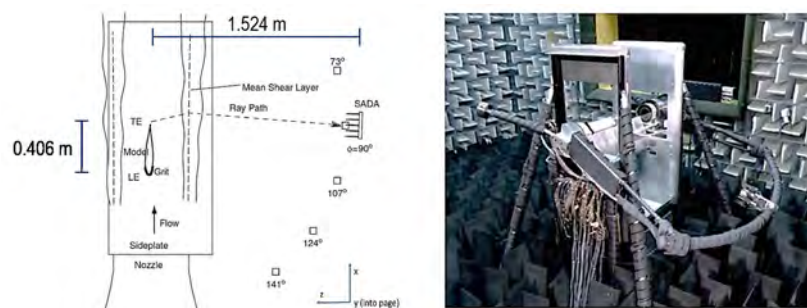


Figure 38: Setup for the Leading Edge/Trailing Edge measurements of the NACA 63-215 Mod-B full-span airfoil in NASA Langley QFF. The airfoil is installed in a clean configuration at its zero-lift angle of attack (-1.2). The coordinate system origin is the center of the nozzle exit plane. Credits: Hutcheson and Brooks

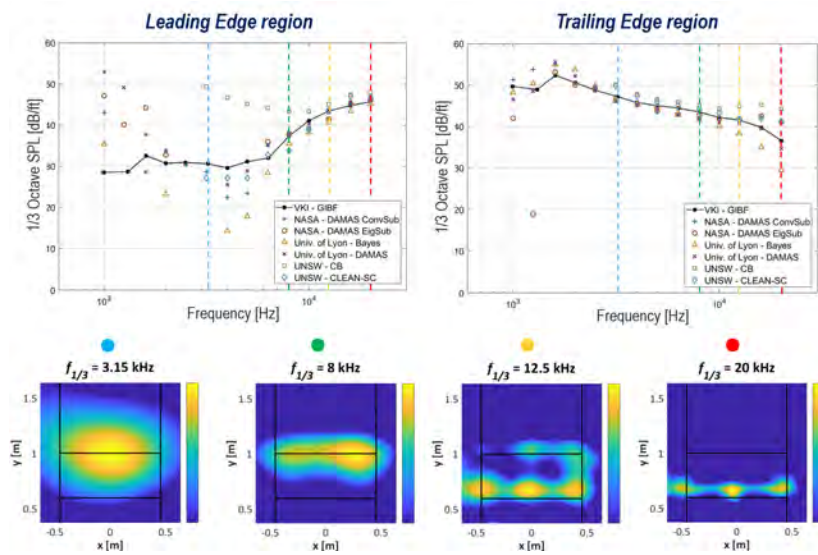


Figure 39: Integrated leading edge and trailing edge one-third octave band spectra per-foot-span computed with various microphone phased array data processing techniques and GIBF noise source distribution maps referred to different one-third octave band frequencies. Credits: Christopher Bahr.

653 *Written by R. Zamponi: riccardo.zamponi@vki.ac.be, von Karman Institute for Fluid Dynamics,*
 654 *Belgium, N. Van de Weyer, von Karman Institute for Fluid Dynamics, Belgium, C. Schram, von*
 655 *Karman Institute for Fluid Dynamics, Belgium*
 656 **Submission Country: Belgium**

657 *7.10. Velocity-Potential Boundary-Field Integral Formulation for Sound Scattered by Moving*
 658 *Bodies*

659 A novel boundary-field integral formulation suitable for the prediction of noise scattered by
 660 moving bodies has been developed and validated in Ref. [85] in the framework of potential
 661 subsonic potential flows. It allows for the appraisal of the role of nonlinear terms in the acoustic
 662 scattering computations for those configurations where the nonuniform mean-flow past the
 663 scattering body is not negligible. Such an issue is not trivial because it is proven that, starting
 664 from the same flow modeling assumptions, linear formulations based on the wave equation for
 665 the velocity potential or on the Lighthill equation and the Ffowcs Williams and Hawkings equation
 666 for the pressure disturbance, provide different predictions when the scatterer is not at rest.
 667 Hence, discrepancies reside in the different influence of the neglected nonlinear terms. The new
 668 velocity potential-based approach is developed by extracting the first-order contributions from
 669 the nonlinear terms. This yields a linearized boundary-field, frequency-domain formulation for
 670 the scattered potential, that extends the standard linear boundary integral approach. The influence
 671 of the additional field contributions is examined for different scatterer velocities, with the
 672 aim of assessing the domain of validity of the fully linear formulation and the rate of grow of the
 673 field contributions with increase of velocity. Specifically, the numerical investigation concerns
 674 the noise scattered by a moving, non-lifting wing, when impinged by an acoustic disturbance
 675 generated by a co-moving point source.

676 *Written by M. Gennaretti (m.gennaretti@uniroma3.it), G. Bernardini, C. Poggi, Roma Tre Uni-*
677 *versity, Italy and C. Testa CNR-INM, Italy.*

678 **Submission Country: Italy**

679 **8. Miscellaneous topics**

680 *8.1. Vehicle Cabin Noise*

681 An important part of the noise inside vehicle cabins is emitted from window vibration. The
682 vibration is excited both hydrodynamically (due to exterior flow impingement on windows) and
683 acoustically (due to exterior flow-induced noise). The flows induced by side-view mirrors up-
684 stream of the windows can significantly contribute to the excitation. As a simplification of a mir-
685 ror, a hemisphere embedded in free stream was investigated using large eddy simulation (LES)
686 [86]. The wake was found to contain predominant exterior noise sources. Furthermore, wake
687 impingement was explored by placing a quarter-spherocylinder blunt body (termed the generic
688 side-view mirror) on a plate (Fig. 40) in a study on cavity interior noise using LES coupled
689 with a finite element method [87]. The analysis of wavenumber-frequency spectra addressed the
690 inhomogeneous feature of surface pressure fluctuations, of which the hydrodynamic component
691 has bent spectral energy ridges due to the inhomogeneous mean convection. The flow inhom-
692 geneity, however, has less influence on the noise magnitude distribution at natural frequencies,
693 as compared to the mode shapes of the window and cavity (Fig. 41). In addition, the efficiencies
694 of the hydrodynamic and acoustic components in the interior noise generation were quantified.
695 Since the quality of cabin noise prediction is dependent on the accuracy of the inputs to the
696 prediction (surface pressure fluctuations), a study on CFD methods for exterior flows and noise
697 was motivated regarding compressibility, turbulence modelling including improved delayed de-
698 tached eddy simulation (IDDES) and LES, and grid topology [88]. The compressible IDDES was
699 down-selected based on its comparatively better performance. This method was then applied to
700 simulate real truck side-view mirrors, which are mounted on a simplified truck body [89]. It was
701 identified that intensive surface pressure fluctuations on the window are mainly caused by the
702 impingement of the free shear layers that initiate from the mirrors and A-pillar.

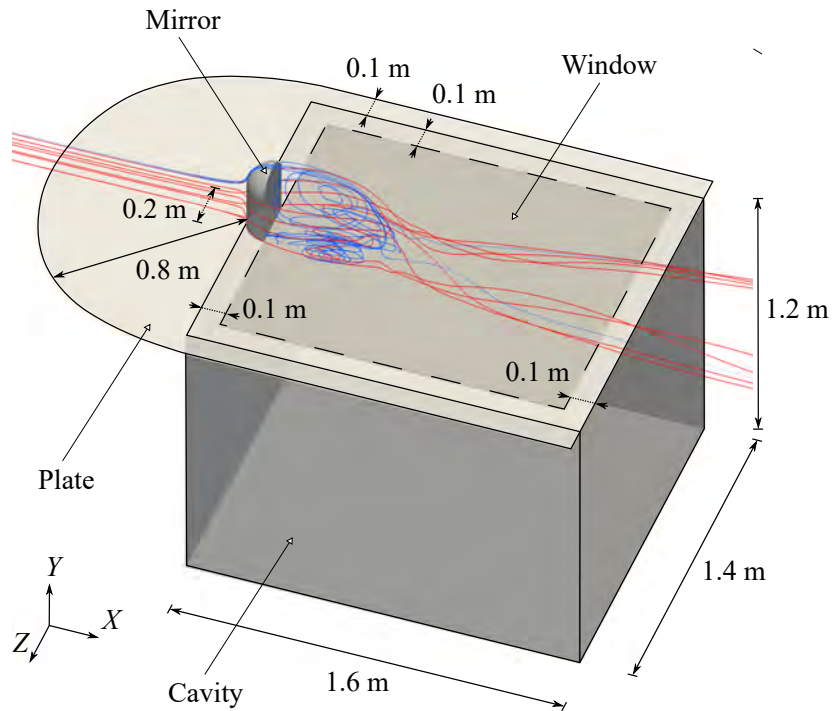


Figure 40: The configuration with streamlines of the time-averaged velocity. The streamlines past the mirror upper edge are colored in blue, and those past the side edges colored in red.

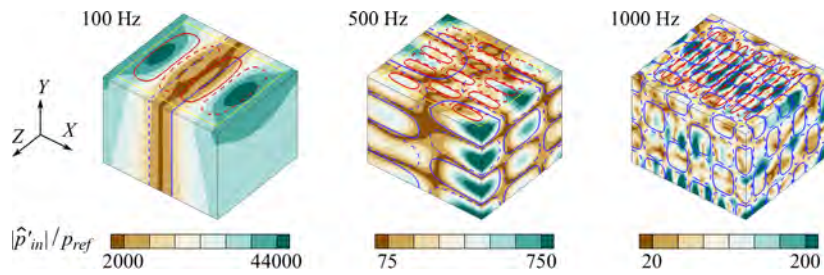


Figure 41: Contours of the interior noise magnitudes at 100Hz, 500Hz, and 1000Hz. From left to right, the red lines show the window mode shapes at 101.6Hz, 503Hz, and 998Hz the blue lines show the cavity mode shapes at 106.3Hz, 501.5Hz, and 1000.4Hz. The solid and dashed line patterns represent the normalized mode shape levels of 0.1 and -0.1, respectively.

703 Written by H.-D. Yao: huadong.yao@chalmers.se, and L. Davidson, Department of Mechanics
 704 and Maritime Sciences, Chalmers University of Technology, Sweden.

705 **Submission Country: Sweden**

707 In-duct multi-microphone measurements are used to determine the acoustic properties of com-
 708 ponents such as acoustic liners. This can involve wave decomposition and determination of scat-
 709 tering matrices. To be able to compare measured results with model predictions, the quality
 710 of the measurements have to be known. Uncertainty analyses are invaluable to assess and im-
 711 prove the quality of measurement results in terms of accuracy and precision. Linear analyses are
 712 widespread, computationally fast and give information of the contribution of each error source to
 713 the overall measurement uncertainty, however they can not be applied in every situation. The pur-
 714 pose of this study was to determine if linear methods can be used to assess the quality of acoustic
 715 scattering matrices. A linear uncertainty analysis was applied to acoustic scattering matrix mea-
 716 surements and the results were compared against Monte-Carlo simulations. It was shown that
 717 a linear uncertainty analysis, applied to the wave decomposition method, gives correct results
 718 for plane waves when three conditions are satisfied. An example of a result, including a 95%
 719 confidence interval, for the reflection coefficient of a rigid wall duct termination can be seen in
 720 Fig 42. When higher order modes are present, the number of conditions that have to be simulta-
 721 neously satisfied increases with the number of cut-on higher order modes and it is better to resort
 722 to a different method. The method was based on matrix perturbation theory, and gives qualitative
 723 information in the form of partial condition numbers and the implementation is straightforward.
 724 Using the alternative method, the measurements of higher order modes were analyzed and the
 725 observed difference in the measured reflection coefficients for different excitation conditions was
 726 explained by the disparity in modal amplitude.

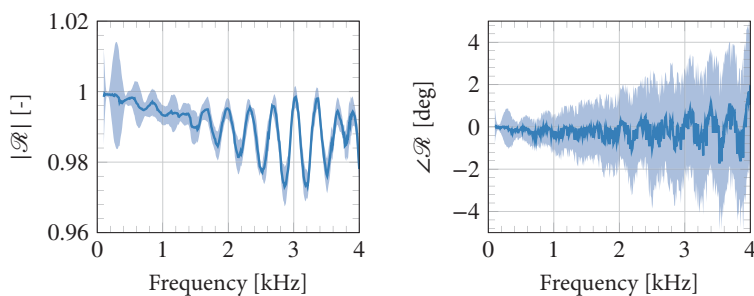


Figure 42: Measured reflection coefficient of a rigid wall with 95% confidence interval. Left absolute value, right phase.

727 Written by Hans Bodén: hansbod@kth.se, KTH, Sweden

728 **Submission Country: Sweden**

729 *8.3. Nonlinear Asymptotic Impedance Model for a Helmholtz Resonator of Finite Depth*

730 In order to model the impedance of an acoustic liner composed of an array of Helmholtz
 731 resonators, a weakly nonlinear theory is developed for the resonance regime of a finite-length
 732 Helmholtz resonator, based on the acoustics of an organ pipe connected to the external excitation
 733 field via an acoustically small neck. The flow through the neck includes linear viscous friction
 734 and nonlinear dissipation due to flow separation and vortex shedding. This paper extends and
 735 refines the previous analysis [90], which considered an acoustically compact cavity.

736 The weakly nonlinear model allows a solution, asymptotic for small, but also moderate, ex-
 737 citation amplitudes. This enables analytically obtaining an expression for the impedance that
 738 includes nonlinear effects for frequencies close to the fundamental resonance frequency.

739 Considering the small number of modelling assumptions, the obtained results compare very
 740 well with experimental data by Motsinger & Kraft [91] in the linear and nonlinear impedance
 741 regimes. See Figure 43

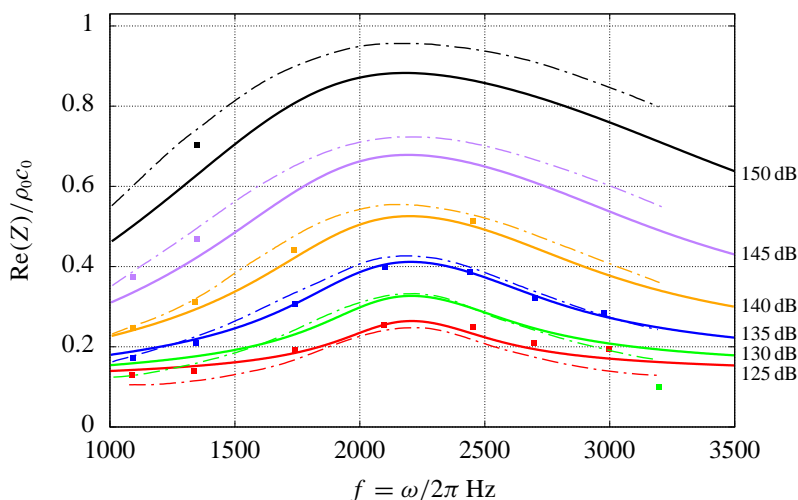


Figure 43: Comparison of impedance resistance $\Re(Z)/\rho_0c_0$, as given by new theory (solid lines), with measurements (squares) and predictions (dash-dotted lines) by Motsinger & Kraft in [91]

742 *Written by Sjoerd W. Rienstra: s.w.rienstra@tue.nl, TUE, The Netherlands and Deepesh Kumar*
 743 *Singh, TUE, The Netherlands, (now: Lilium, Germany)*

744 **Submission Country: The Netherlands**

745 *8.4. Analytical prediction of limit-cycle oscillations amplitude in solid rocket motors*

746 In large Solid Rocket Motors (SRMs), vortex-driven indirect sound leads to the establish-
 747 ment of a feedback loop resulting in self-sustained limit-cycle pressure pulsations [92, 93, 94].
 748 Paramount to this mechanism is the interaction of vortices, created near a geometric feature of
 749 the combustion chamber, with the nozzle as they exit [95]. For vortex-driven self-sustained pres-
 750 sure pulsations, the presence of a cavity around the choked nozzle inlet has been demonstrated
 751 to have a major influence. Indeed, cold-gas experiments of a scale model of the Ariane 5 SRM

752 have shown that the limit-cycle amplitude of vortex- driven self-sustained pressure pulsations
753 are proportional to the nozzle cavity volume [92]. Hirschberg et al. [95] have used dedicated
754 vortex-nozzle interaction simulations, based on a frictionless compressible model proposed by
755 Hulshoff et al. [96], to develop a new scaling law for this indirect sound source. Hirschberg et al.
756 identified key parameters, viz., the nozzle inlet Mach number, the vortex circulation and the dy-
757 namic pressure upstream from the nozzle [95]. Using an energy balance approach, Hirschberg et
758 al. [94] formulated an analytical model which predicts, within an order of magnitude, pulsation
759 amplitudes observed in cold gas-scale experiments of Ariane 5. Both this analytical model and
760 the numerical study of vortex-nozzle interaction, confirmed the importance of the nozzle cavity
761 volume.

762 *Written by Lionel Hirschberg: l.hirschberg@me.com, von Karman Institute for Fluid Dynamics,*
763 *Belgium and Centrale Supélec, France*

764 **Submission Country: Belgium**

765 8.5. *Light Electrospun Polyvinylpyrrolidone Blankets*

766 Traditional sound absorption materials (foams, fibres, membranes, etc..) have good noise re-
767 duction abilities at high frequency range, but exhibit insufficient sound absorption properties in
768 the low and medium frequency range in which human sensitivity to noise is fairly high. There-
769 fore, materials with excellent noise reduction properties in the low and medium frequency range
770 are highly desirable for acoustical purposes. Polymeric soundproofing materials have been fabri-
771 cated by electrospinning polyvinylpyrrolidone (PVP) [97]. The mats were produced in the form
772 of thin disks of 10 cm in diameter with a fibre diameter of (1.6 ± 0.5) or $(2.8 \pm 0.5) \mu m$. The
773 sound absorption coefficients were measured using an impedance tube instrument. For a given
774 set of disks (from a minimum of 6) the sound absorption coefficient changed with the frequency
775 (in the range 200-1600 Hz) following a bell shape curve with a maximum (where the coefficient
776 is greater than 0.9) that shifts to lower frequencies with an increasing number of piled disks
777 and with greater fibre diameter (Fig. 44). The acoustic behaviour can be continuously tuned by
778 changing the mass of the blanket (number of plies).

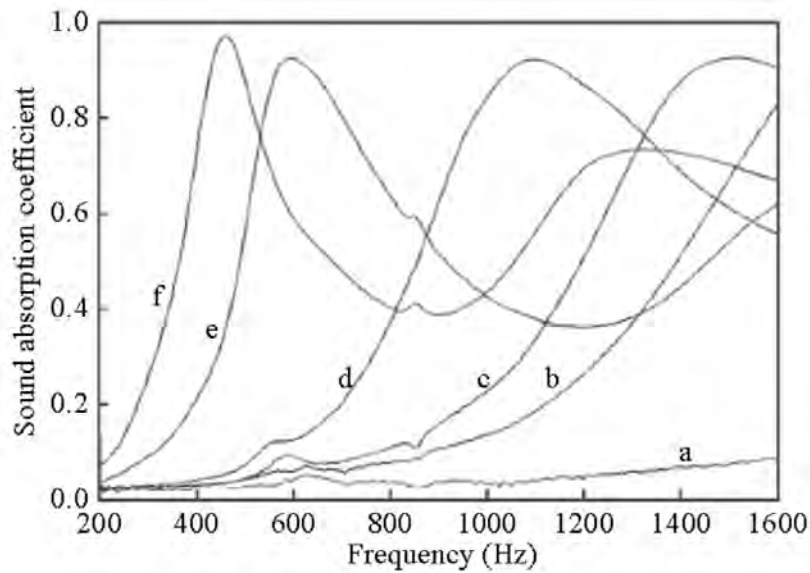


Figure 44: Sound absorption coefficient as a function of frequency for various β disk piles. Curves a, b, c, d, e and f refer, respectively, to samples β_1 , β_{1-4} , β_{1-6} , β_{1-10} , β_{1-17} and β_{1-22} , (β_{i-j} means the pile made of all disks from the i -th to j -th

779 Moreover, in view to improve flame retardancy that often, because of very severe regulations
 780 (as in aerospace engineering), prevents the applicability of materials, the addition of graphene
 781 in the PVP blanket has been considered [97, 98] and the sound absorption coefficient has been
 782 evaluated for different concentrations [[99]]. Results, reported in Fig. 45 for a PVP blanket
 783 (mass of about 7.5 ± 0.5 g), reveal that the addition of graphene does not lower the very high
 784 sound absorption coefficient value but it affects, in a non-monotonous manner, the bell shaped
 785 curves versus frequency becoming sharper and moving to higher frequency at the lower graphene
 786 addition. The opposite is observed when the graphene content is further increased.

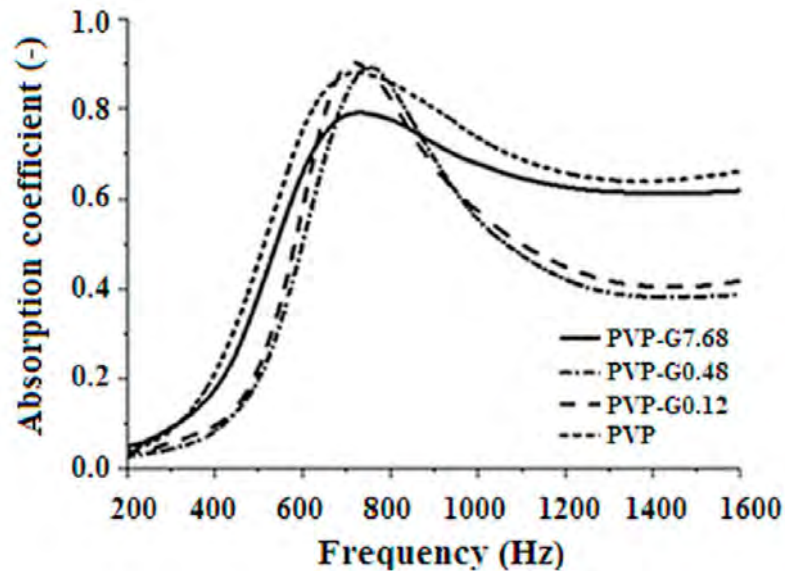


Figure 45: Comparison of sound absorption coefficient as a function of frequency of PVP blankets without and with the addition of graphene of different concentrations

787 *Written by Giuseppe Petrone (giuseppe.petrone@unina.it), Francesco Marulo, Francesco*
 788 *Branda, University of Naples Federico II, Italy*
 789 **Submission Country: Italy**

790 References

- 791 [1] S. Péron, T. Renaud, M. Terracol, C. Benoit, I. Mary, An immersed boundary method for preliminary design aero-
 792 dynamic studies of complex configurations, in: 23rd AIAA Computational Fluid Dynamics Conference, volume
 793 (3623).
 794 [2] S. Redonnet, S. Ben Khelil, J. Bulté, G. Cunha, Numerical characterization of landing gear aeroacoustics using
 795 advanced simulation and analysis techniques, *Journal of Sound and Vibration* 403 (2017) 214 – 233.
 796 [3] D. C. Mincu, T. Le Garrec, S. Peron, M. Terracol, Immersed boundary conditions for high order caa solvers-
 797 aeroacoustics installation effects assessment, in: 23rd AIAA/CEAS Aeroacoustics Conference, 3504.
 798 [4] J. Wickerhoff, T. Sijpkens, Aeroplane provided with noise-reducing means, as well as a landing gear and blowing
 799 means (2004).
 800 [5] S. Oerlemans, A. de Bruin, Reduction of Landing Gear Noise Using an Air Curtain, in: 15th AIAA/CEAS Aero-
 801 acoustics Conference (30th AIAA Aeroacoustics Conference), American Institute of Aeronautics and Astronautics,
 802 Miami, Florida, 2009.
 803 [6] K. Zhao, X.-x. Yang, P. N. Okolo, W.-h. Zhang, Gareth J. Bennett, Use of a plane jet for flow-induced noise
 804 reduction of tandem rods, *Chinese Physics B* 25 (2016) 064301–1 – 064301–9.
 805 [7] Kun Zhao, Patrick N Okolo, John Kennedy, Gareth J Bennett, A study of planar jet flow control and perforated
 806 fairings for the reduction of the flow-induced noise of tandem rods in a cross-flow (AIAA2016-2772), in: 22nd
 807 AIAA/CEAS Aeroacoustics Conference, AIAA, Lyon, France, 2016.
 808 [8] K. Zhao, S. Alimohammadi, P. N. Okolo, J. Kennedy, G. J. Bennett, Aerodynamic noise reduction using dual-jet
 809 planar air curtains, *Journal of Sound and Vibration* 432 (2018) 192–212.
 810 [9] K. Zhao, X. Yang, P. N. Okolo, Z. Wu, G. J. Bennett, Use of dual planar jets for the reduction of flow-induced
 811 noise, *AIP Advances* 7 (2017) 025312–1 – 025312–7.

- 812 [10] K. Zhao, P. N. Okolo, Y. Wang, J. Kennedy, G. J. Bennett, An Experimental Characterization of the Interaction
813 Between Two Tandem Planar Jets in a Crossflow, *Journal of Fluids Engineering* 140 (2018) 111106–1 – 111106–
814 12.
- 815 [11] K. Zhao, P. N. Okolo, J. Kennedy, G. J. Bennett, 2D PIV measurement on the interaction zone between two parallel
816 planar jets in a crossflow, *AIP Advances* 7 (2017) 105104–1 – 105104–21.
- 817 [12] K. Zhao, X. Yang, P. N. Okolo, Z. Wu, W. Zhang, G. J. Bennett, A Novel Method for Defining the Leeward Edge
818 of the Planar Jet in Crossflow, *Journal of Applied Fluid Mechanics* 10 (2017) 1475–1486.
- 819 [13] Gareth J. Bennett, Patrick N. Okolo, Kun Zhao, John Philo, Yaoyi Guan, Scott C. Morris, Cavity Resonance
820 Suppression Using Fluidic Spoilers, *AIAA Journal* 57 (2018) 706–719.
- 821 [14] Eleonora Neri, John Kennedy, Massimiliano Di Giulio, Ciaran O’Reilly, Jeremy Dahan, Marco Esposito, Massi-
822 miliano Bruno, Francesco Amoroso, Antonello Bianco, Gareth J. Bennett, Characterization of Low Noise Tech-
823 nologies Applied to a Full Scale Fuselage Mounted Nose Landing Gear, in: *Internoise2015: Proceedings of the*
824 *Internoise 2015/ASME NCAD Meeting*, American Society of Mechanical Engineers, San Francisco, CA, USA,
825 2015, pp. Paper No: NCAD2015–5911.
- 826 [15] Eleonora Neri, John Kennedy, Gareth J. Bennett, Aeroacoustic Source Separation on a Full Scale Nose Landing
827 Gear Featuring Combinations of Low Noise Technologies, in: *Internoise2015: Proceedings of the Internoise*
828 *2015/ASME NCAD Meeting*, American Society of Mechanical Engineers, San Francisco, CA, USA, 2015, pp.
829 Paper No: NCAD2015–5912.
- 830 [16] Petr Eret, John Kennedy, Gareth J. Bennett, Effect of noise reducing components on nose landing gear stability for
831 a mid-size aircraft coupled with vortex shedding and freeplay, *Journal of Sound and Vibration* 354 (2015) 91–103.
- 832 [17] Gareth J. Bennett, Eleonora Neri, John Kennedy, Noise Characterization of a Full-Scale Nose Landing Gear,
833 *Journal of Aircraft* 55 (2018) 2476 – 2490.
- 834 [18] Eleonora Neri, John Kennedy, Gareth J. Bennett, Bay cavity noise for full-scale nose landing gear: A comparison
835 between experimental and numerical results, *Aerospace Science and Technology* 72 (2018) 278–291.
- 836 [19] Gareth J. Bennett, David B. Stephens, Francisco Rodriguez Verdugo, Resonant mode characterisation of a cylin-
837 drical Helmholtz cavity excited by a shear layer, *The Journal of the Acoustical Society of America* 141 (2017)
838 7–18.
- 839 [20] Roberto Merino Martinez, Eleonora Neri, Mirjam Snellen, John Kennedy, Dick Simons, Gareth J. Bennett, Analy-
840 sis of nose landing gear noise comparing numerical computations, prediction models and flyover and wind-tunnel
841 measurements, in: *24th AIAA/CEAS Aeroacoustics Conference*, American Institute of Aeronautics and Astronau-
842 tics, Georgia, Atlanta, USA, 2018.
- 843 [21] John Kennedy, Elenora Neri, Gareth J. Bennett, The Reduction of Main Landing Gear Noise (AIAA 2016-2900),
844 in: *22nd AIAA/CEAS Aeroacoustics Conference*, Lyon, France.
- 845 [22] Saloua Ben Khelil, Philippe Bardoux, Jean-Luc Godard, Thomas Le Garrec, John Kennedy, Gareth J. Bennett,
846 Investigation of the Noise Emission of a Regional Aircraft Main Landing Gear Bay, in: *23rd AIAA/CEAS Aeroa-*
847 *coustics Conference*, American Institute of Aeronautics and Astronautics, Denver, Colorado, USA, 2017.
- 848 [23] S. R. Koh, B. Zhou, M. Meinke, N. Gauger, W. Schröder, Numerical analysis of the impact of variable porosity on
849 trailing-edge noise, *Computers & Fluids* 167 (2018) 66–81.
- 850 [24] S. R. Koh, M. Meinke, W. Schröder, Numerical analysis of the impact of permeability on trailing-edge noise,
851 *Journal of Sound and Vibration* 421 (2018) 348–376.
- 852 [25] R. Amiet, Noise due to turbulent flow past a trailing edge, *Journal of Sound and Vibration* 47 (1976) 387–393.
- 853 [26] R. L. Panton, J. H. Linebarger, Wall pressure spectra calculations for equilibrium boundary layers, *Journal of Fluid*
854 *Mechanics* 65 (1974) 261.
- 855 [27] S. Lee, Empirical wall-pressure spectral modeling for zero and adverse pressure gradient flows, *AIAA Journal* 56
856 (2018) 1818–1829.
- 857 [28] D.-Y. Maa, Potential of microperforated panel absorbers, *Journal of the Acoustical Society of America* 104 (1998)
858 2861–2866.
- 859 [29] C. Maury, T. Bravo, D. Mazzoni, The use of microperforations to attenuate the cavity pressure fluctuations induced
860 by a low-speed flow, *Journal of Sound and Vibration* 439 (2019) 1–16.
- 861 [30] F. Avallone, W. Van Der Velden, D. Ragni, D. Casalino, Noise reduction mechanisms of sawtooth and combed-
862 sawtooth trailing-edge serrations, *Journal of Fluid Mechanics* 848 (2018).
- 863 [31] D. Ragni, F. Avallone, W. van der Velden, D. Casalino, Measurements of near-wall pressure fluctuations for
864 trailing-edge serrations and slits, *Experiments in Fluids* 60 (2019) 6.
- 865 [32] D. Casalino, F. Avallone, I. Gonzalez-Martino, D. Ragni, Aeroacoustic study of a wavy stator leading edge in a
866 realistic fan/OGV stage, *Journal of Sound and Vibration* 442 (2019) 138–154.
- 867 [33] F. Avallone, D. Casalino, D. Ragni, Impingement of a propeller-slipstream on a leading edge with a flow-permeable
868 insert: A computational aeroacoustic study, *International Journal of Aeroacoustics* 17 (2018) 687–711.
- 869 [34] A. Rubio Carpio, R. Merino-Martínez, F. Avallone, D. Ragni, M. Snellen, S. van der Zwaag, Experimental char-
870 acterization of the turbulent boundary layer over a porous trailing edge for noise abatement, *Journal of Sound and*

- 871 Vibration 443 (2019) 537–558.
- 872 [35] M. Kopiev, V. Zaytsev, D. Akhmetov, V. Nikulin, Aerodynamic noise generated by large-scale vortex ring, in:
873 25th International Congress of Sound and Vibration (ICSV 25).
- 874 [36] D. G. Achmetov, *Vortex rings*, Springer, Berlin, 2009. OCLC: 492248946.
- 875 [37] V. F. Kopiev, S. A. Chernyshev, Vortex ring eigen-oscillations as a source of sound, *Journal of Fluid Mechanics*
876 341 (1997) 19–57.
- 877 [38] M. Daroukh, C. Polacsek, A. Chelius, Shockwave Generation and Radiation from an UHBR Engine with Flow Dis-
878 tortion using a CFD/CAA Coupling Strategy, in: To appear (accepted abstract) in 25th AIAA/CEAS Aeroacoustics
879 Conference, Delft, The Netherlands.
- 880 [39] L. Cambier, S. Heib, S. Plot, The Onera elsA CFD software: input from research and feedback from industry,
881 *Mechanics & Industry* 14 (2013) 159–174.
- 882 [40] J. Thisse, C. Polacsek, J. Mayeur, S. Khelladi, X. Gloerfelt, A. Lafitte, Numerical Simulations of Shock-Wave
883 Propagation in Turbofan Intakes, in: In 22nd AIAA/CEAS Aeroacoustics Conference, Lyon, France.
- 884 [41] A. Pereira, J. Regnard, E. Salze, F. Gea-Aguilera, M. Gruber, New modular fan rig for advanced aeroacoustic
885 tests - modal decomposition on a 20° UHBR fan stage, in: Proceedings of the 25th AIAA/CEAS Aeroacoustics
886 Conference, Delft, Netherlands.
- 887 [42] C. Brandstetter, B. Paoletti, X. Ottavy, Compressible modal instability onset in an aerodynamically mistuned
888 transonic fan, *Journal of Turbomachinery* 141 (2019) 031004.
- 889 [43] Q. Leclre, A. Pereira, C. Bailly, J. Antoni, C. Picard, A unified formalism for acoustic imaging based on microphone
890 array measurements, *International Journal of Aeroacoustics* 16 (2017) 431–456.
- 891 [44] A. J. K. C. S. M. M. Shur, M. Strelets, Effect of inlet distortions on ducted fan noise, Proceedings of the 22nd
892 AIAA/CEAS Aeroacoustics Conference (2016).
- 893 [45] R. J. Dominique, J. Christophe, C. Schram, Multi-port eduction of installation effects applied to a small axial fan,
894 *Acta Acustica united with Acustica* 105 (2019) 75–85.
- 895 [46] J. Lavrentjev, M. bom, Characterization of fluid machines as acoustic multi-port sources, *Journal of Sound and*
896 *Vibration* 197 (1996) 1–16.
- 897 [47] J. C. Tyacke, Z.-N. Wang, P. G. Tucker, LES–RANS of installed ultra-high-bypass-ratio coaxial jet aeroacoustics
898 with flight stream, *AIAA Journal* (2018) 1–22.
- 899 [48] Z.-N. Wang, J. Tyacke, P. Tucker, P. Boehning, Parallel computation of aeroacoustics of industrially relevant
900 complex-geometry aeroengine jets, *Computers & Fluids* 178 (2019) 166–178.
- 901 [49] J. C. Tyacke, Z.-N. Wang, P. G. Tucker, Noise source, length and time scale distributions in installed jets with a
902 flight stream, in: 2018 AIAA/CEAS Aeroacoustics Conference, p. 3619.
- 903 [50] S. Modini, G. Graziani, G. Bernardini, M. Gennaretti, Pressure feedback-based blade–vortex interaction noise
904 controller for helicopter rotors, *International Journal of Aeroacoustics* 17 (2018) 295–318.
- 905 [51] S. Modini, G. Graziani, G. Bernardini, M. Gennaretti, Blade-vortex interaction noise controller based on miniature
906 trailing edge effectors., *International Journal of Acoustics & Vibration* 23 (2018).
- 907 [52] M. Gennaretti, G. Bernardini, J. Serafini, G. Romani, Rotorcraft comprehensive code assessment for blade–vortex
908 interaction conditions, *Aerospace Science and Technology* 80 (2018) 232–246.
- 909 [53] G. Bernardini, J. Serafini, M. M. Colella, M. Gennaretti, Analysis of a structural-aerodynamic fully-coupled
910 formulation for aeroelastic response of rotorcraft, *Aerospace Science and Technology* 29 (2013) 175–184.
- 911 [54] A. V. Smol'yakov, V. M. Tkachenko, Models of a field of pseudosound turbulent wall pressures and experimental
912 data, *Akust. Zh* 37 (1991) 1199–1207.
- 913 [55] A. Klages, Aircraft fuselage vibration excitation by turbulent boundary layer flow in cruise, Ph.D. thesis, Institute
914 of Aerodynamics and Flow Technology, German Aerospace Center, 2017.
- 915 [56] N. Hu, S. Callsen, A parametric study on wall pressure wavenumber-spectrum models with application to aircraft
916 fuselage vibration prediction, 26th International Congress on Sound and Vibration (2019).
- 917 [57] Gareth J. Bennett, John Kennedy, Petr Eret, Filippo Cappadona, Antonello Bianco, Raffaele Letizia, Davide Danise,
918 Lucille Lamotte, Christophe Picard, Arthur Finez, Paolo Castellini, Paolo Chiariotti, Francesca Sopranzetti, De-
919 mosthenis Tsahalis, Haralabos Tsahalis, Vassilios Moussas, Antonio Paonessa, Francesco Amoroso, Massimiliano
920 Di Giulio, WENEMOR: Wind Tunnel Tests for the Evaluation of the Installation Effects of Noise Emissions of
921 an Open Rotor Advanced Regional Aircraft (AIAA 2013-2092), in: 19th AIAA/CEAS Aeroacoustics Conference
922 (32nd AIAA Aeroacoustics Conference), American Institute of Aeronautics and Astronautics, Berlin, Germany,
923 2013.
- 924 [58] John Kennedy, Petr Eret, Gareth J. Bennett, Paolo Castellini, Paolo Chiariotti, Francesca Sopranzetti, Christophe
925 Picard, Arthur Finez, The application of advanced beamforming techniques for the noise characterization of in-
926 stalled counter rotating open rotors (AIAA 2013-2093), in: 19th AIAA/CEAS Aeroacoustics Conference (32nd
927 AIAA Aeroacoustics Conference), American Institute of Aeronautics and Astronautics, Berlin, Germany, 2013.
- 928 [59] John Kennedy, Petr Eret, Gareth J. Bennett, A parametric study of installed counter rotating open rotors (AIAA
929 2013-2094), in: 19th AIAA/CEAS Aeroacoustics Conference (32nd AIAA Aeroacoustics Conference), American

- Institute of Aeronautics and Astronautics, Berlin, Germany, 2013.
- [60] J Kennedy, P Eret, Gareth J. Bennett, A parametric study of airframe effects on the noise emission from installed contra-rotating open rotors, *International Journal of Aeroacoustics* 17 (2018) 624–654.
- [61] P. Eret, J. Kennedy, F. Amoroso, P. Castellini, Gareth J. Bennett, Experimental observations of an installed-on-pylon contra-rotating open rotor with equal blade number in pusher and tractor configuration, *International Journal of Aeroacoustics* 15 (2016) 228–249.
- [62] L Sanders, D-C Mincu, PI Vitagliano, M Minervino, J Kennedy, G Bennett, Prediction of the acoustic shielding by aircraft empennage for contra-rotating open rotors, *International Journal of Aeroacoustics* 16 (2017) 626–648.
- [63] Laurent Sanders, Daniel C. Mincu, Williams Denis, Pier Luigi Vitagliano, Mauro Minervino, John Kennedy, Petr Eret, Gareth J. Bennett, A coupling of computational methods for CROR installation effects (AIAA 2014-3190), in: *AIAA Aviation, 20th AIAA/CEAS Aeroacoustics Conference*, American Institute of Aeronautics and Astronautics, Atlanta, GA, USA, 2014.
- [64] C. Horvth, B. Fenyvesi, B. Kocsis, M. Quaglia, S. Moreau, J. Kennedy, G. J. Bennett, Towards counter-rotating open rotor noise reduction via radiation efficiency considerations, in: *25th AIAA/CEAS Aeroacoustics Conference*, American Institute of Aeronautics and Astronautics, Delft, The Netherlands, 2019.
- [65] V. F. Kopiev, S. A. Chernyshev, *Methods of the Lagrangian and Hamiltonian Mechanics in Aeroacoustics Problems*, *Acoustical Physics* 64 (2018) 707–717.
- [66] O. Jiříček, Aeroacoustics research in Europe: The CEAS-ASC report on 2015 highlights, *Journal of Sound and Vibration* 381 (2016) 101–120.
- [67] V. Fleury, R. Davy, Analysis of jetairfoil interaction noise sources by using a microphone array technique, *Journal of Sound and Vibration* 364 (2016) 44–66.
- [68] T. Brooks, W. Humphreys, A deconvolution approach for the mapping of acoustic sources (damas) determined from phased microphone arrays, *Journal of Sound and Vibration* 294 (2006) 856–879.
- [69] S. Fauqueux, R. Davy, Modal deconvolution method in a finite circular duct, using flush-mounted microphones, in: *24th AIAA/CEAS Aeroacoustics Conference*, AIAA, Atlanta, Georgia, 2018.
- [70] M. Laban, J. Kok, H. Brouwer, Cfd/caa analysis of uhbr engine tonal noise, in: *24th AIAA/CEAS Aeroacoustics Conference*, AIAA, Atlanta, Georgia, 2018.
- [71] T. Kuhn, J. Dürrwächter, A. Beck, C.-D. Munz, F. Meyer, C. Rohde, Uncertainty quantification for direct aeroacoustic simulations of cavity flows, *Journal of Theoretical and Computational Acoustics* (2018).
- [72] M. Moessner, C. Kissner, J. Delfs, L. Enghardt, Computational chain for virtual fly-over simulations applied to fan noise, in: *24th AIAA/CEAS Aeroacoustics Conference*.
- [73] C. Kissner, S. Guérin, L. Enghardt, H. Siller, M. Pott-Pollenske, The Challenge of Tonal Fan Noise Prediction for an Aircraft Engine in Flight, *Acta Acustica united with Acustica* 105 (2019) 17–29.
- [74] S. Luesutthiviboon, A. M. N. Malgoezar, R. Merino-Martinez, M. Snellen, P. Sijtsma, D. G. Simons, Enhanced HR-CLEAN-SC for resolving multiple closely-spaced sound sources, *International Journal of Aeroacoustics* (2019). Accepted for publication.
- [75] P. Sijtsma, CLEAN based on spatial source coherence, *International Journal of Aeroacoustics* 6 (2007) 357–374.
- [76] P. Sijtsma, R. Merino-Martinez, A. M. N. Malgoezar, M. Snellen, High-Resolution CLEAN-SC: Theory and Experimental Validation, *International Journal of Aeroacoustics* 16 (2017) 274–298.
- [77] R. Merino-Martinez, E. Neri, M. Snellen, J. Kennedy, D. Simons, G. Bennett, Analysis of nose landing gear noise comparing numerical computations, prediction models and flyover and wind-tunnel measurements, in: *24th AIAA/CEAS Aeroacoustics Conference*. June 25 – 29 2018. Atlanta, Georgia, USA. AIAA paper 2018–3299.
- [78] M. G. Jones, W. R. Watson, T. L. Parrott, Benchmark data for evaluation of aeroacoustic propagation codes with grazing flow, *AIAA paper 2853* (2005) 2005.
- [79] J. Primus, E. Piot, F. Simon, An adjoint-based method for liner impedance education: Validation and numerical investigation, *Journal of Sound and Vibration* 332 (2013) 58–75.
- [80] R. Roncen, F. Méry, E. Piot, F. Simon, Statistical inference method for liner impedance education with a shear grazing flow, *AIAA Journal* (2018) 1–11.
- [81] F. Monteghetti, D. Matignon, E. Piot, L. Pascal, Design of broadband time-domain impedance boundary conditions using the oscillatory-diffusive representation of acoustical models, *Journal of the Acoustical Society of America* 140 (2016) 1663–1674.
- [82] F. Monteghetti, D. Matignon, E. Piot, Energy analysis and discretization of nonlinear impedance boundary conditions for the time-domain linearized euler equations, *Journal of Computational Physics* 375 (2018) 393–426.
- [83] T. Suzuki, L1 generalized inverse beam-forming algorithm resolving coherent/incoherent, distributed and multipole sources, *Journal of Sound and Vibration* 330 (2011) 5835–5851.
- [84] C. J. Bahr, W. M. Humphreys, D. Ernst, T. Ahlefeldt, C. Spehr, A. Pereira, Q. Leclre, C. Picard, R. Porteous, D. Moreau, J. R. Fischer, C. J. Doolan, A Comparison of Microphone Phased Array Methods Applied to the Study of Airframe Noise in Wind Tunnel Testing, in: *23rd AIAA/CEAS Aeroacoustics Conference*, American Institute

- 988 of Aeronautics and Astronautics, Denver, Colorado, 2017.
- 989 [85] M. Gennaretti, G. Bernardini, C. Poggi, C. Testa, Velocity-potential boundary-field integral formulation for sound
990 scattered by moving bodies, *AIAA Journal* 56 (2018) 3547–3557.
- 991 [86] H.-D. Yao, L. Davidson, Noise radiated by low-Reynolds number flows past a hemisphere at $Ma=0.3$, *Physics of*
992 *Fluids* 29(7) (2017) 076102.
- 993 [87] H.-D. Yao, L. Davidson, Generation of interior cavity noise due to window vibration excited by turbulent flows
994 past a generic side-view mirror, *Physics of Fluids* 30 (2018) 036104.
- 995 [88] H.-D. Yao, L. Davidson, Z. Chron er, Investigation of interior noise from generic side-view mirror using incom-
996 pressible and compressible solvers of DES and LES, *SAE Technical Paper* (2018) 2018–01–0735.
- 997 [89] H.-D. Yao, L. Davidson, Z. Chron er, Simplifications applied for simulation of turbulence induced by a side view
998 mirror of a full-scale truck using DES, *SAE Technical Paper* (2018) 2018–01–0708.
- 999 [90] Sjoerd W. Rienstra, Deepesh Kumar Singh, Nonlinear asymptotic impedance model for a Helmholtz resonator
1000 liner, *Journal of Sound and Vibration* 333 (2014) 3536–3549.
- 1001 [91] R.E. Motsinger, R.E. Kraft, Design and Performance of Duct Acoustic Treatment, *Acoustical Society of America*,
1002 pp. 165–206.
- 1003 [92] J r me Anthoine, Jean-Marie Buchlin, Avraham Hirschberg, Effect of nozzle cavity on resonance in large SRM:
1004 Theoretical modeling, *Journal of Propulsion and Power* 18 (2002) 304–311.
- 1005 [93] S. Gallier, M. Prevost, J. Hijlkema, M. Roumy, Effects of cavity on thrust oscillations in subscale solid rocket
1006 motors, in: 45th AIAA/ASME/SAE/ASEE Joint Propulsion Conference & Exhibit, p. 5253.
- 1007 [94] Lionel Hirschberg, Thierry Schuller, Jean Collinet, Christophe Schram, Avraham Hirschberg, Analytical model
1008 for the prediction of pulsations in a cold-gas scale-model of a Solid Rocket Motor, *Journal of Sound and Vibration*
1009 419 (2018) 452–468.
- 1010 [95] L. Hirschberg, S. Hulshoff, J. Collinet, C. Schram, T. Schuller, Vortex nozzle interaction in solid rocket motors:
1011 A scaling law for upstream acoustic response, *The Journal of the Acoustical Society of America* 144 (2018)
1012 EL46–EL51.
- 1013 [96] S. Hulshoff, A. Hirschberg, G. Hofmans, Sound production of vortex–nozzle interactions, *Journal of Fluid Me-*
1014 *chanics* 439 (2001) 335–352.
- 1015 [97] J. Avossa, F. Branda, F. Marulo, G. Petrone, S. Guido, G. Tomaiuolo, A. Costantini, Light electrospun
1016 polyvinylpyrrolidone blanket for low frequencies sound absorption, *Chinese Journal of Polymer Science (English*
1017 *Edition)* 36 (2018) 1368–1374.
- 1018 [98] G. Del Sorbo, G. Truda, A. Bifulco, J. Passaro, G. Petrone, B. Vitolo, G. Ausanio, A. Vergara, F. Marulo, F. Branda,
1019 Non monotonous effects of noncovalently functionalized graphene addition on the structure and sound absorption
1020 properties of polyvinylpyrrolidone (1300 kda) electrospun mats, *Materials* 12 (2018).
- 1021 [99] F. Branda, F. Marulo, S. Guido, G. Petrone, G. Del Sorbo, G. Truda, G. Tomaiuolo, Polyvinylpyrrolidone (pvp) /
1022 graphene based soundproofing materials through electrospinning, volume 2017-January.